Northumbria
University
NEWCASTLE

Nonlinear static and transient isogeometric analysis of functionally graded microplates based on the modified strain gradient theory

Son Thai[a], Huu-Tai Thai[b,c,a,*], Thuc P. Vo[d,e], H. Nguyen-Xuan[f]

[a]*School of Engineering and Mathematical Sciences, La Trobe University, Bundoora, VIC 3086, Australia*
[b]*Division of Construction Computation, Institute for Computational Science, Ton Duc Thang University, Ho Chi Minh City, Vietnam*
[c]*Faculty of Civil Engineering, Ton Duc Thang University, Ho Chi Minh City, Vietnam*
[d]*Institute of Research and Development, Duy Tan University, 03 Quang Trung, Da Nang, Vietnam*
[e]*Department of Mechanical and Construction Engineering, Northumbria University, Ellison Place, Newcastle upon Tyne NE1 8ST, UK*
[f]*Center for Interdisciplinary Research in Technology (CIRTech), Hutech University, Ho Chi Minh City 700000, Vietnam*

Abstract

The objective of this study is to develop an effective numerical model within the framework of an isogeometric analysis (IGA) to investigate the geometrically nonlinear responses of functionally graded (FG) microplates subjected to static and dynamic loadings. The size effect is captured based on the modified strain gradient theory with three length scale parameters. The third-order shear deformation plate theory is adopted to represent the kinematics of plates, while the geometric nonlinearity is accounted based on the von Kármán assumption. Moreover, the variations of material phrases through the plate thickness follow the rule of mixture. By using Hamilton's principle, the governing equation of motion is derived and then discretized based on the IGA technique, which tailors the non-uniform rational B-splines (NURBS) basis functions as interpolation functions to fulfil the C^2-continuity requirement. The nonlinear equations are solved by the Newmark's time integration scheme with Newton-Raphson iterative procedure. Various examples are also presented to study the influences of size effect, material variations, boundary conditions and shear deformation on the nonlinear behaviour of FG microplates.

Keywords: Isogeometric Analysis; Modified strain gradient theory; Geometrical nonlinearity; Functionally graded microplate

1. Introduction

In recent years, there has been a considerable increase in research and applications of functionally graded materials (FGMs) in various engineering fields. FGMs are categorized as a class of composite materials [1] since they are constituted from two or more phrases of distinct materials. Those constituent materials in FGMs are varied intentionally and continuously through a prescribed

*Corresponding author. E-mail: thaihuutai@tdt.edu.vn (H.T. Thai)

dimension, and hence there is no stress concentration as observed in conventional laminated composites. Ceramic and metal constituents are the most common material phrases from which FGMs are commonly made. In general, the ceramic constituent has a strong capability to withstand a high-temperature effect, whereas the metal counterpart is able to exhibit robust mechanical properties due to its ductility. By combining those constituents with smooth variations of their volume fractions, the preferable mechanical characteristics of both materials are obtained in a unique structure. Thanks to this distinguishing feature, it is no doubt that FGMs have also been studied for applications in cutting-edge devices [2] in whcih microbeams and microplates are fundamental components. In the mechanical point of view, the behaviour of such microstructures is considerably influenced by the size effect as indicated in various experimental investigations [3–5]. In addition, it was pointed out that the classical elasticity theory is incapable of predicting accurately the responses of the small-scale structures. This is due to the fact that the classical elasticity theory lacks a so-called length scale parameter, which is used to capture the size effect. To deal with this shortage, a number of non-classical continuum theories were proposed in the open literature, such as the strain gradient theory of Mindlin [6], the nonlocal elasticity theory of Eringen [7], the nonlocal strain gradient theory [8], the modified couple stress theory (MCT) of Yang et al. [9] and the modified strain gradient elasticity theory (MST) of Lam et al. [10]. The adoption of those theories to study the behaviour of small-scale structures could be found in various studies on nano/microbeams [11–17] nano/microplates [18–28] or nanoshells [29–31]. A critical review of recent research on the application of nonclassical continuum theories for predicting the size-dependent behaviour of small-scale structures can be also found in [32].

Based on the MST, a number of size-dependent models have been developed to predict the responses of microplates on the basis of various kinematic models, such as classical plate theory [33–37], first-order shear deformation theory [38–43] and higher-order shear deformation theories [44–47]. However, these aforementioned works are limited to analytical or semi-analytical methods, which are only applicable to simple problems with certain geometry and boundary and loading conditions. For example, Wang et al. [33], Sahmani and Ansari [44], Gholami et al. [40], Zhang et al. [41, 46] and Akgoz and Civalek [47] employed Navier method to derive analytical solutions of rectangular microplates with simply supported boundary conditions, whilst Mohammadi and Fooladi Mahani [35] and Mohammadi et al. [36] used Levy method to derive analytical solutions of rectangular microplates in which two opposite edges are simply supported and the remaning two edges can have arbitrary boundary conditions. The behaviour of microplates with various boundary conditions were also studied using semi-analytical methods such as the differential quadrature method

[38, 39, 42, 43, 45] and the extended Kantorovich method [34, 37]. For the practical problems with complex geometries, loadings and boundary conditions, the application of analytical methods to solve such problems is impossible due to the mathematical complexity of the MST plate models. Therefore, numerical approaches such as finite element method, finite strip method, Ritz method become the most suitable candidates for solving such problems. However, the adoption of classical and high-order shear deformation theories would pose an obstacle for the traditional finite element method as they require a continuity of interpolation functions over the element boundaries. This difficulty is naturally and efficiently handled by using the IGA technique [48], in which the NURBS basis functions are not only smooth and highly continuous but also able to present exact geometries of some conical objects [49–52].

Although numerical solutions of the MST models have been recently developed using Chebyshev-Ritz method [53], the finite strip method [54] and the IGA method [55], these studies were limited to linear problems (linear bending [55], linear buckling [54] and linear free vibration [53, 54]). In fact, the behaviour of microplates could undergo large deformations when heavier loads are imposed. Therefore, the geometrical nonlinearity should be considered in the analyses of microplates. However, no literature has been reported for the nonlinear analysis of FG micropaltes based on the MST except a recent study on post-buckling of microplates conducted by Thai et al. [56]. Therefore, the aim of this paper is to propose an effective numerical approach to predict the geometrically nonlinear responses of FG microplates based on the MST and the IGA approach. The displacement field is based on the third-order shear deformation theory of Reddy [57], while the geometrical nonlinearity is accounted by adopting the von Kármán assumption. Hamilton's principle is utilized to construct the weak form of the equation of motion. In addition, the NURBS basis functions are employed as interpolation functions to satisfy the C^2-continuity requirement in the discretization process. The Newmark's integration scheme in conjunction with Newton-Rhapson iterative procedure is adopted for the nonlinear static and dynamic analysis. Verification studies are also performed to prove the accuracy of the present approach. The influences of the size effect, material gradient indices, boundary conditions and thickness ratios on the nonlinear responses of FG microplates are firstly investigated through various parametric studies.

2. Plate formulations

2.1. Material properties of FGMs

As described in Fig. 1, the in-plane coordinates x and y are located in the midplane Ω of the plate having the thickness of h, while the z-axis is normal to the midplane. According to the rule of

mixture, the variation of material properties throughout the plate thickness is expressed by

$$P\left(z\right)=\left(P_c-P_m\right)\left(\frac{z}{h}+\frac{1}{2}\right)^n+P_m \tag{1}$$

where $P(z)$ is a typical material property, such as Young's modulus $E(z)$, Poisson's ratio $\nu(z)$, density $\rho(z)$. P_c and P_m represent the properties of ceramic and metal surfaces, respectively, and the gradient index n is used to describe the profile of material variation. It can be seen that a single ceramic or metal plate is obtained when the gradient index n is prescribed as 0 or ∞.

2.2. Modified strain gradient theory

Based on the MST proposed by Lam et al. [10], the virtual strain energy stored in an elastic body is expressed as

$$\delta U=\int\limits_V\left(\sigma_{ij}\delta\varepsilon_{ij}+p_i\delta\varsigma_i+\tau_{ijk}^{(1)}\delta\eta_{ijk}^{(1)}+m_{ij}^s\delta\chi_{ij}^s\right)\mathrm{d}V \tag{2}$$

where the classical stress and high-order stresses are given as follows

$$\sigma_{ij}=2\mu\varepsilon_{ij}+\lambda\varepsilon_{kk}\delta_{ij};\ p_i=2\mu l_0^2\varsigma_i;\ \tau_{ijk}^{(1)}=2\mu l_1^2\eta_{ijk}^{(1)};\ m_{ij}^s=2\mu l_2^2\chi_{ij}^s \tag{3}$$

in which l_0, l_1 and l_2 are the material length scale parameters. λ and μ denote the Lamé constants:

$$\lambda=\frac{\nu E(z)}{\left[1+\nu(z)\right]\left[1-2\nu(z)\right]};\ \ \mu=\frac{E(z)}{2\left[1+\nu(z)\right]} \tag{4}$$

The classical strain tensor ε_{ij} and high-order strain gradient tensors, namely the dilatation gradient tensor ζ_i, the deviatoric stretch gradient tensor $\eta_{ijk}^{(1)}$ and the symmetric part of rotation gradient tensor χ_{ij}^s, are given as follows

$$\varepsilon_{ij}=\frac{1}{2}\left(u_{i,j}+u_{j,i}+u_{m,i}u_{m,j}\right); \tag{5a}$$

$$\varsigma_i=\varepsilon_{mm,i} \tag{5b}$$

$$\eta_{ijk}^{(1)}=\eta_{ijk}^s-\frac{1}{5}\left(\delta_{ij}\eta_{mmk}^s+\delta_{jk}\eta_{mml}^s+\delta_{ki}\eta_{mmj}^s\right);\ \eta_{ijk}^s=\frac{1}{3}\left(u_{i,jk}+u_{j,ki}+u_{k,ij}\right) \tag{5c}$$

$$\chi_{ij}^s=\frac{1}{4}\left(e_{imn}u_{n,mj}+e_{jmn}u_{n,mi}\right) \tag{5d}$$

where u_i denote the components of displacement vector, δ_{ij} and e_{ijk} are the Kronocker delta and permutation symbol, respectively.

2.3. Kinematics

The displacement field according to the third-order shear deformation plate theory [57] is expressed as follows

$$\begin{aligned}u_1&=u+f\left(z\right)\theta_x-g\left(z\right)w_{,x}\\u_2&=v+f\left(z\right)\theta_y-g\left(z\right)w_{,y}\\u_3&=w\end{aligned} \tag{6}$$

where (u, v, w) and (θ_x, θ_y) are the displacements and rotations of an arbitrary point in the midplane, and $f(z) = z - 4z^3/3h^2;\ g(z) = 4z^3/3h^2$.

By substituting Eq. (6) into Eq. (5) and adopting the von Kármán assumption, the strain-displacement relations are obtained as follows

For the classical strains

$$\boldsymbol{\varepsilon} = \boldsymbol{\varepsilon}_0 + \frac{1}{2}\boldsymbol{\varepsilon}_{nl} + f(z)\,\boldsymbol{\varepsilon}_1 + g(z)\,\boldsymbol{\varepsilon}_2 \tag{7a}$$

$$\boldsymbol{\gamma} = f'(z)\,\boldsymbol{\gamma}_1 + (1 - g'(z))\,\boldsymbol{\gamma}_2 \tag{7b}$$

For the dilatation gradient strains

$$\boldsymbol{\varsigma} = \boldsymbol{\varsigma}_0 + \boldsymbol{\varsigma}_{nl} + f(z)\,\boldsymbol{\varsigma}_1 + g(z)\,\boldsymbol{\varsigma}_2 \tag{8a}$$

$$\varsigma_z = f'(z)\,\varsigma_3 + g'(z)\,\varsigma_4 \tag{8b}$$

For the deviatoric stretch gradient strains

$$\boldsymbol{\eta} = \boldsymbol{\eta}_0 + \boldsymbol{\eta}_{nl} + f''(z)\,\boldsymbol{\eta}_1 + f'(z)\,\boldsymbol{\eta}_2 + f(z)\,\boldsymbol{\eta}_3 + g''(z)\,\boldsymbol{\eta}_4 + g'(z)\,\boldsymbol{\eta}_5 + g(z)\,\boldsymbol{\eta}_6 \tag{9}$$

For the symmetric part of rotation gradient strains

$$\boldsymbol{\chi} = \boldsymbol{\chi}_0 + f''(z)\,\boldsymbol{\chi}_1 + f'(z)\,\boldsymbol{\chi}_2 + f(z)\,\boldsymbol{\chi}_3 + g''(z)\,\boldsymbol{\chi}_4 + g'(z)\,\boldsymbol{\chi}_5 \tag{10}$$

The linear components in above expressions can be found in [55], whilst the additional nonlinear components are given as follows

$$\boldsymbol{\varsigma}_{nl} = \begin{Bmatrix} w_{,x}w_{,xx} + w_{,y}w_{,xy} \\ w_{,x}w_{,xy} + w_{,y}w_{,yy} \end{Bmatrix} \tag{11a}$$

$$\boldsymbol{\varsigma}_{nl} = \begin{Bmatrix} w_{,x}w_{,xx} + w_{,y}w_{,xy} \\ w_{,x}w_{,xy} + w_{,y}w_{,yy} \end{Bmatrix} \tag{11b}$$

$$\boldsymbol{\eta}_{nl} = \begin{Bmatrix} \frac{2}{5}w_{,x}w_{,xx} - \frac{1}{5}w_{,x}w_{,yy} - \frac{2}{5}w_{,y}w_{,xy} \\ -\frac{2}{5}w_{,x}w_{,xy} - \frac{1}{5}w_{,y}w_{,xx} + \frac{2}{5}w_{,y}w_{,yy} \\ 0 \\ \frac{8}{15}w_{,x}w_{,xy} + \frac{4}{15}w_{,y}w_{,xx} - \frac{1}{5}w_{,y}w_{,yy} \\ 0 \\ -\frac{1}{5}w_{,x}w_{,xx} + \frac{4}{15}w_{,x}w_{,yy} + \frac{8}{15}w_{,y}w_{,xy} \\ 0 \\ -\frac{1}{5}w_{,x}w_{,xx} - \frac{1}{15}w_{,x}w_{,yy} - \frac{2}{15}w_{,y}w_{,xy} \\ 0 \\ -\frac{2}{15}w_{,x}w_{,xy} - \frac{1}{15}w_{,y}w_{,xx} - \frac{1}{5}w_{,y}w_{,yy} \end{Bmatrix} \tag{11c}$$

Herein, the prime notation denotes the derivative with respect to z. It is seen that the nonlinear components are involved in the classical strain tensor, dilatation gradient tensor and deviatoric stretch gradient tensor. However, there is no nonlinear component in the symmetric part of rotation gradient tensor. This also signifies the superior feature of the MST over the MCT on the nonlinear analyses of microstructures.

The constitutive relations are obtained as follows

$$\hat{\boldsymbol{\sigma}} = \begin{Bmatrix} \mathbf{N}^{\varepsilon} \\ \mathbf{M}^{\varepsilon} \\ \mathbf{L}^{\varepsilon} \\ \mathbf{T}^{\varepsilon} \\ \mathbf{U}^{\varepsilon} \end{Bmatrix} = \begin{bmatrix} \mathbf{A}^{\varepsilon} & \mathbf{P}^{\varepsilon} & \mathbf{C}^{\varepsilon} & \mathbf{0} & \mathbf{0} \\ \mathbf{P}^{\varepsilon} & \mathbf{H}^{\varepsilon} & \mathbf{F}^{\varepsilon} & \mathbf{0} & \mathbf{0} \\ \mathbf{C}^{\varepsilon} & \mathbf{F}^{\varepsilon} & \mathbf{G}^{\varepsilon} & \mathbf{0} & \mathbf{0} \\ \mathbf{0} & \mathbf{0} & \mathbf{0} & \bar{\mathbf{A}}^{\varepsilon} & \bar{\mathbf{P}}^{\varepsilon} \\ \mathbf{0} & \mathbf{0} & \mathbf{0} & \bar{\mathbf{P}}^{\varepsilon} & \bar{\mathbf{C}}^{\varepsilon} \end{bmatrix} \left(\begin{Bmatrix} \boldsymbol{\varepsilon}_0 \\ \boldsymbol{\varepsilon}_1 \\ \boldsymbol{\varepsilon}_2 \\ \boldsymbol{\varepsilon}_3 \\ \boldsymbol{\varepsilon}_4 \end{Bmatrix} + \frac{1}{2} \begin{Bmatrix} \boldsymbol{\varepsilon}_{nl} \\ \mathbf{0} \\ \mathbf{0} \\ \mathbf{0} \\ \mathbf{0} \end{Bmatrix} \right) = \hat{\mathbf{D}}_{\varepsilon} \left(\hat{\boldsymbol{\varepsilon}} + \hat{\boldsymbol{\varepsilon}}_{nl} \right) \quad (12a)$$

$$\hat{\mathbf{p}} = \begin{Bmatrix} \mathbf{N}^{\varsigma} \\ \mathbf{M}^{\varsigma} \\ \mathbf{L}^{\varsigma} \\ \mathbf{T}^{\varsigma} \\ \mathbf{U}^{\varsigma} \end{Bmatrix} = \begin{bmatrix} A^{\varsigma} & P^{\varsigma} & C^{\varsigma} & 0 & 0 \\ P^{\varsigma} & H^{\varsigma} & F^{\varsigma} & 0 & 0 \\ C^{\varsigma} & F^{\varsigma} & G^{\varsigma} & 0 & 0 \\ 0 & 0 & 0 & \bar{A}^{\varsigma} & \bar{P}^{\varsigma} \\ 0 & 0 & 0 & \bar{P}^{\varsigma} & \bar{C}^{\varsigma} \end{bmatrix} \left(\begin{Bmatrix} \boldsymbol{\varsigma}_0 \\ \boldsymbol{\varsigma}_1 \\ \boldsymbol{\varsigma}_2 \\ \boldsymbol{\varsigma}_3 \\ \boldsymbol{\varsigma}_4 \end{Bmatrix} + \begin{Bmatrix} \boldsymbol{\varsigma}_{nl} \\ \mathbf{0} \\ \mathbf{0} \\ \mathbf{0} \\ \mathbf{0} \end{Bmatrix} \right) = \hat{\mathbf{D}}_{\varsigma} \left(\hat{\boldsymbol{\varsigma}} + \hat{\boldsymbol{\varsigma}}_{nl} \right) \quad (12b)$$

$$\hat{\boldsymbol{\tau}} = \begin{Bmatrix} \mathbf{N}^{\eta} \\ \mathbf{M}^{\eta} \\ \mathbf{L}^{\eta} \\ \mathbf{T}^{\eta} \\ \mathbf{S}^{\eta} \\ \mathbf{U}^{\eta} \\ \mathbf{R}^{\eta} \end{Bmatrix} = \begin{bmatrix} A^{\eta} & P^{\eta} & C^{\eta} & Q^{\eta} & \bar{P}^{\eta} & \bar{C}^{\eta} & \bar{Q}^{\eta} \\ P^{w} & H^{\eta} & F^{\eta} & Y^{\eta} & \bar{H}^{\eta} & \bar{F}^{\eta} & \bar{Y}^{\eta} \\ C^{w} & F^{\eta} & G^{\eta} & Z^{\eta} & \bar{K}^{\eta} & \bar{G}^{\eta} & \bar{Z}^{\eta} \\ Q^{w} & Y^{\eta} & Z^{\eta} & W^{\eta} & \bar{I}^{\eta} & \bar{J}^{\eta} & \bar{W}^{\eta} \\ \bar{P}^{w} & \bar{H}^{\eta} & \bar{K}^{\eta} & \bar{I}^{\eta} & \widehat{K}^{\eta} & \bar{B}^{\eta} & \bar{O}^{\eta} \\ \bar{C}^{w} & \bar{F}^{\eta} & \bar{G}^{\eta} & \bar{J}^{\eta} & \bar{B}^{\eta} & \widehat{I}^{\eta} & \bar{E}^{\eta} \\ \bar{Q}^{w} & \bar{Y}^{\eta} & \bar{Z}^{\eta} & \bar{W}^{\eta} & \bar{O}^{\eta} & \bar{E}^{\eta} & \widehat{J}^{\eta} \end{bmatrix} \left(\begin{Bmatrix} \boldsymbol{\eta}_0 \\ \boldsymbol{\eta}_1 \\ \boldsymbol{\eta}_2 \\ \boldsymbol{\eta}_3 \\ \boldsymbol{\eta}_4 \\ \boldsymbol{\eta}_5 \\ \boldsymbol{\eta}_6 \end{Bmatrix} + \begin{Bmatrix} \boldsymbol{\eta}_{nl} \\ \mathbf{0} \\ \mathbf{0} \\ \mathbf{0} \\ \mathbf{0} \\ \mathbf{0} \\ \mathbf{0} \end{Bmatrix} \right) = \hat{\mathbf{D}}_{\eta} \left(\hat{\boldsymbol{\eta}} + \hat{\boldsymbol{\eta}}_{nl} \right) \quad (12c)$$

$$\hat{\mathbf{m}} = \begin{Bmatrix} \mathbf{N}^{\chi} \\ \mathbf{M}^{\chi} \\ \mathbf{L}^{\chi} \\ \mathbf{T}^{\chi} \\ \mathbf{S}^{\chi} \\ \mathbf{U}^{\chi} \end{Bmatrix} = \begin{bmatrix} A^{\chi} & P^{\chi} & C^{\chi} & Q^{\chi} & \bar{P}^{\chi} & \bar{C}^{\chi} \\ P^{\chi} & H^{\chi} & F^{\chi} & Y^{\chi} & \bar{H}^{\chi} & \bar{F}^{\chi} \\ C^{\chi} & F^{\chi} & G^{\chi} & Z^{\chi} & \bar{K}^{\chi} & \bar{G}^{\chi} \\ Q^{\chi} & Y^{\chi} & Z^{\chi} & W^{\chi} & \bar{I}^{\chi} & \bar{J}^{\chi} \\ \bar{P}^{\chi} & \bar{H}^{\chi} & \bar{K}^{\chi} & \bar{I}^{\chi} & \widehat{K}^{\chi} & \bar{B}^{\chi} \\ \bar{C}^{\chi} & \bar{F}^{\chi} & \bar{G}^{\chi} & \bar{J}^{\chi} & \bar{B}^{\chi} & \widehat{I}^{\chi} \end{bmatrix} \begin{Bmatrix} \boldsymbol{\chi}_0 \\ \boldsymbol{\chi}_1 \\ \boldsymbol{\chi}_2 \\ \boldsymbol{\chi}_3 \\ \boldsymbol{\chi}_4 \\ \boldsymbol{\chi}_5 \end{Bmatrix} = \hat{\mathbf{D}}_{\chi} \hat{\boldsymbol{\chi}} \quad (12d)$$

in which definitions of stress resultants and component of constitutive matrices are presented in details in [55].

Based on the small strain assumption, the equation of motion without damping effect obtained from Hamilton's principle can be expressed with respect to the initial configuration by

$$\int_{\Omega} \delta\left(\hat{\boldsymbol{\varepsilon}}+\frac{1}{2}\hat{\boldsymbol{\varepsilon}}_{nl}\right)^{T}\hat{\mathbf{D}}_{\varepsilon}\left(\hat{\boldsymbol{\varepsilon}}+\frac{1}{2}\hat{\boldsymbol{\varepsilon}}_{nl}\right)\mathrm{d}\Omega+\int_{\Omega}\delta(\hat{\boldsymbol{\varsigma}}+\hat{\boldsymbol{\varsigma}}_{nl})^{T}\hat{\mathbf{D}}_{\varsigma}\left(\hat{\boldsymbol{\varsigma}}+\hat{\boldsymbol{\varsigma}}_{nl}\right)\mathrm{d}\Omega+$$
$$\int_{\Omega}\delta(\hat{\boldsymbol{\eta}}+\hat{\boldsymbol{\eta}}_{nl})^{T}\hat{\mathbf{D}}_{\eta}\boldsymbol{\Gamma}_{\eta}\left(\hat{\boldsymbol{\eta}}+\hat{\boldsymbol{\eta}}_{nl}\right)\mathrm{d}\Omega+\int_{\Omega}\delta\hat{\boldsymbol{\chi}}^{T}\hat{\mathbf{D}}_{\chi}\boldsymbol{\Gamma}_{\chi}\hat{\boldsymbol{\chi}}\mathrm{d}\Omega+\int_{\Omega}\delta\tilde{\mathbf{u}}^{T}\mathbf{m}\ddot{\tilde{\mathbf{u}}}\mathrm{d}\Omega=\int_{\Omega}q\delta w\mathrm{d}\Omega \quad (13)$$

where $\tilde{\mathbf{u}}=\left\{\begin{array}{ccc}\tilde{\mathbf{u}}_1 & \tilde{\mathbf{u}}_2 & \tilde{\mathbf{u}}_3\end{array}\right\}^{T}$ with

$$\tilde{\mathbf{u}}_1=\left\{\begin{array}{c}u\\v\\w\end{array}\right\};\tilde{\mathbf{u}}_2=\left\{\begin{array}{c}\theta_x\\\theta_y\\0\end{array}\right\};\tilde{\mathbf{u}}_3=\left\{\begin{array}{c}-w_{,x}\\-w_{,y}\\0\end{array}\right\} \quad (14)$$

$\mathbf{m}$ denotes the mass matrix, which is expressed by

$$\mathbf{m}=\left[\begin{array}{ccc}I_1 & I_2 & I_3\\I_3 & I_4 & I_5\\I_3 & I_5 & I_6\end{array}\right] \quad (15)$$

where

$$\left(I_1,I_2,I_3,I_4,I_5,I_6\right)=\int_{-h/2}^{h/2}\rho_e\left(z\right)\left(1,f\left(z\right),g\left(z\right),\left(f\left(z\right)\right)^2,f\left(z\right)g\left(z\right),\left(g\left(z\right)\right)^2\right)\mathrm{d}z \quad (16)$$

$\boldsymbol{\Gamma}_{\eta}$ and $\boldsymbol{\Gamma}_{\chi}$ are diagonal matrices of coefficients as given below

$$diag\left(\boldsymbol{\Gamma}_{\eta}\right)=\left\{\begin{array}{cccccccccc}1 & 1 & 1 & 3 & 3 & 3 & 6 & 1 & 1 & 1\end{array}\right\} \quad (17a)$$

$$diag\left(\boldsymbol{\Gamma}_{\chi}\right)=\left\{\begin{array}{cccccc}1 & 1 & 2 & 1 & 2 & 2\end{array}\right\} \quad (17b)$$

3. Solution procedure

3.1. IGA-based plate model

In this study, the IGA approach is employed to solve MST problems due to its computational efficiency compared to tranditional finite element method [49]. The idea of this approach was proposed Hughes et al. [48] by using the same basis functions for representing the geometry in Computed-Aided Design (CAD) models and approximating the physical fields and state variables in the Finite Element Analysis (FEA). In this method, the B-splines basis function of degree p is constructed based on a so-called knot vector, which is defined as a set of parameters $\Xi=\{\xi_1,\xi_2,\xi_3,...,\xi_i,...,\ \xi_{n+p+1}\}$, $\xi_i\leq$

ξ_{i+1} with n denoting the number of generated basis functions [58]. By using the Cox-de Boor formula, the B-spline basis functions $N_{i,0}(\xi)$ are recursively generated starting with $p = 0$

$$N_{i,0}(\xi) = \begin{cases} 1 & \xi_i \leq \xi < \xi_{i+1} \\ 0 & \text{otherwise} \end{cases} \tag{18}$$

and then, for $p \geq 1$,

$$N_{i,p} = \frac{\xi - \xi_i}{\xi_{i+p} - \xi_i} N_{i,p-1}(\xi) + \frac{\xi_{i+p+1} - \xi}{\xi_{i+p+1} - \xi_{i+1}} N_{i,p-1}(\xi) \tag{19}$$

The B-splines basis functions are $C^{\infty}-$continuous inside a knot span and $C^{p-k}-$continuous at the knots having multiplicity of k. This distinguishing feature makes the B-splines basis functions superior to the interpolation functions of traditional FEA. An example of the B-splines basis functions is depicted in Fig. 2.

For 2-D problems, the NURBS basis functions $R^{p,q}_{i,j}(\xi, \eta)$ are constructed from two univariate B-spline basis functions $N_{i,p}(\xi)$ and $M_{j,q}(\eta)$ according to a tensor product:

$$R^{p,q}_{i,j}(\xi, \eta) = \frac{N_{i,p}(\xi) M_{i,q}(\eta) w_{i,j}}{\sum_{\hat{i}=1}^{n} \sum_{\hat{j}=1}^{m} N_{\hat{i},p}(\xi) M_{\hat{j},q}(\eta) w_{\hat{i},\hat{j}}} \tag{20}$$

where $w_i > 0$ are the weight coefficients.

By employing the NURBS basis functions as the interpolation functions, the displacement variables are expressed by

$$\bar{\mathbf{u}} = \sum_{c}^{m \times n} R_c(\xi, \eta) \mathbf{d}_c \tag{21}$$

where $\bar{\mathbf{u}} = \begin{bmatrix} u & v & \theta_x & \theta_y & w \end{bmatrix}^T$, $\mathbf{d}_c = \begin{bmatrix} u_c & v_c & \theta_{xc} & \theta_{yc} & w_c \end{bmatrix}^T$ is the vector consisting degree of freedoms corresponding to the control point c, $m \times n$ denotes the numbers of control points associated with an element. By using Eq. (21), the strain tensor and other gradient tensors can be expressed as follows

$$\hat{\boldsymbol{\varepsilon}} = \sum_{c}^{m \times n} \mathbf{B}_{\varepsilon c} \mathbf{d}_c = \sum_{c}^{m \times n} \begin{Bmatrix} \mathbf{B}^0_{\varepsilon} \\ \mathbf{B}^1_{\varepsilon} \\ \mathbf{B}^2_{\varepsilon} \\ \mathbf{B}^3_{\varepsilon} \\ \mathbf{B}^4_{\varepsilon} \end{Bmatrix}_c \mathbf{d}_c; \;\; \hat{\boldsymbol{\varsigma}} = \sum_{c}^{m \times n} \mathbf{B}_{\varsigma c} \mathbf{d}_c = \sum_{c}^{m \times n} \begin{Bmatrix} \mathbf{B}^0_{\varsigma} \\ \mathbf{B}^1_{\varsigma} \\ \mathbf{B}^2_{\varsigma} \\ \mathbf{B}^3_{\varsigma} \\ \mathbf{B}^4_{\varsigma} \end{Bmatrix}_c \mathbf{d}_c; \tag{22a}$$

$$\hat{\boldsymbol{\eta}} = \sum_{c}^{m\times n} \mathbf{B}_{\eta c}\mathbf{d}_c = \sum_{c}^{m\times n} \left\{ \begin{array}{c} \mathbf{B}_{\eta}^{0} \\ \mathbf{B}_{\eta}^{1} \\ \mathbf{B}_{\eta}^{2} \\ \mathbf{B}_{\eta}^{3} \\ \mathbf{B}_{\eta}^{4} \\ \mathbf{B}_{\eta}^{5} \\ \mathbf{B}_{\eta}^{6} \end{array} \right\}_c \mathbf{d}_c;\ \hat{\boldsymbol{\chi}} = \sum_{c}^{m\times n} \mathbf{B}_{\chi c}\mathbf{d}_c = \sum_{c}^{m\times n} \left\{ \begin{array}{c} \mathbf{B}_{\chi}^{0} \\ \mathbf{B}_{\chi}^{1} \\ \mathbf{B}_{\chi}^{2} \\ \mathbf{B}_{\chi}^{3} \\ \mathbf{B}_{\chi}^{4} \\ \mathbf{B}_{\chi}^{5} \end{array} \right\}_c \mathbf{d}_c \tag{22b}$$

$$\boldsymbol{\varepsilon}_{nl} = \mathbf{B}_{\varepsilon nl}\mathbf{d} = \sum_{c}^{m\times n} \boldsymbol{\Lambda}_{\varepsilon c}\mathbf{B}_{gc}\mathbf{d}_c;\ \boldsymbol{\varsigma}_{nl} = \mathbf{B}_{\varsigma nl}\mathbf{d} = \sum_{c}^{m\times n} \boldsymbol{\Lambda}_{\varsigma c}\mathbf{B}_{gc}\mathbf{d}_c;\ \boldsymbol{\eta}_{nl} = \mathbf{B}_{\eta nl}\mathbf{d} = \sum_{c}^{m\times n} \boldsymbol{\Lambda}_{\eta c}\mathbf{B}_{gc}\mathbf{d}_c \tag{22c}$$

in which $\mathbf{B}_{\varepsilon}^{i}, \mathbf{B}_{\varsigma}^{i}, \mathbf{B}_{\eta}^{i}$ and $\mathbf{B}_{\chi}^{i}$ are the linear strain-displacement matrices given in [55]. Details of additional nonlinear components are provided in the Appendix.

Substituting Eqs. (22) into Eq. (13), the NURBS-based formulation for the equation of motion is expressed as

$$\left(\mathbf{K}_{\varepsilon} + \mathbf{K}_{\varsigma} + \mathbf{K}_{\eta} + \mathbf{K}_{\chi}\right)\mathbf{d} + \mathbf{M}\ddot{\mathbf{d}} = \mathbf{f} \tag{23}$$

in which the double dot subscript denotes the second derivative with respect to time. $\mathbf{K}_{\varepsilon}, \mathbf{K}_{\varsigma}, \mathbf{K}_{\eta}$ and $\mathbf{K}_{\chi}$ are the stiffness matrices corresponding to the strain tensor ε_{ij}, the dilatation gradient tensor ς_i, the deviatoric stretch gradient tensor $\eta_{ijk}^{(1)}$ and the symmetric part of rotation gradient tensor χ_{ij}^{s}, respectively. $\mathbf{M}$ and $\mathbf{f}$ denote the global mass matrix and load vector. Expressions for the stiffness matrices are given by

$$\mathbf{K}_{\varepsilon} = \int_{\Omega} \left(\mathbf{B}_{\varepsilon T}^{T}\hat{\mathbf{D}}\mathbf{B}_{\varepsilon} + \frac{1}{2}\mathbf{B}_{\varepsilon T}^{T}\hat{\mathbf{D}}\mathbf{B}_{\varepsilon nl} + \mathbf{B}_{\varepsilon nl}^{T}\hat{\mathbf{D}}\mathbf{B}_{\varepsilon} + \frac{1}{2}\mathbf{B}_{\varepsilon nl}^{T}\hat{\mathbf{D}}\mathbf{B}_{\varepsilon nl} \right) \mathrm{d}\Omega \tag{24a}$$

$$\mathbf{K}_{\varsigma} = \int_{\Omega} \left(\mathbf{B}_{\varsigma T}^{T}\hat{\mathbf{D}}_{\varsigma}\mathbf{B}_{\varsigma} + \mathbf{B}_{\varsigma T}^{T}\hat{\mathbf{D}}_{\varsigma}\mathbf{B}_{\varsigma nl} + \mathbf{B}_{\varsigma nl}^{T}\hat{\mathbf{D}}_{\varsigma}\mathbf{B}_{\varsigma} + \mathbf{B}_{\varsigma nl}^{T}\hat{\mathbf{D}}_{\varsigma}\mathbf{B}_{\varsigma}^{nl} + \mathbf{B}_{g}^{T}\hat{\mathbf{N}}_{\varsigma}\mathbf{B}_{g\varsigma} \right) \mathrm{d}\Omega \tag{24b}$$

$$\mathbf{K}_{\eta} = \int_{\Omega} \left(\mathbf{B}_{\eta T}^{T}\boldsymbol{\Gamma}_{\eta}\hat{\mathbf{D}}_{\eta}\mathbf{B}_{\eta} + \mathbf{B}_{\eta T}^{T}\boldsymbol{\Gamma}_{\eta}\hat{\mathbf{D}}_{\eta}\mathbf{B}_{\eta nl} + \mathbf{B}_{\eta nl}^{T}\boldsymbol{\Gamma}_{\eta}\hat{\mathbf{D}}_{\eta}\mathbf{B}_{\eta} + \mathbf{B}_{\eta nl}^{T}\boldsymbol{\Gamma}_{\eta}\hat{\mathbf{D}}_{\eta}\mathbf{B}_{\eta nl} + \mathbf{B}_{g}^{T}\hat{\mathbf{N}}_{\eta}\mathbf{B}_{g\eta} \right) \mathrm{d}\Omega \tag{24c}$$

$$\mathbf{K}_{\chi} = \int_{\Omega} \mathbf{B}_{\chi}^{T}\hat{\mathbf{D}}_{\chi}\boldsymbol{\Gamma}_{\chi}\mathbf{B}_{\chi}\mathbf{d}\mathrm{d}\Omega \tag{24d}$$

In the MST plate models based on the third-order shear deformation theory, the third-order derivatives of basis functions are required to construct the stiffness matrices. As a result, the basis functions should be C^2-continuous. This demand is not a trivial task in the framework of traditional FEA. However, with the introduction of advanced $k-$ refinement technique [58], the continuity of basis functions in the IGA approach is easily and naturally elevated. In order to fulfil the C^2-continuity demand, the basis functions with order of $p \geq 3$ are adopted in this study.

3.2. Nonlinear analysis

The Newton-Rapshon iterative scheme is employed herein to obtain the solution of nonlinear problems [59]. A brief review of the procedure is given as follows. At the i^{th} iteration, the residual vector $\mathbf{R}$ and the global tangent stiffness matrix are calculated as

$$\mathbf{R}\left(\mathbf{d}^{(i)}\right) = \mathbf{K}\left(\mathbf{d}^{(i)}\right)\mathbf{d}^{(i)} - \mathbf{f} \tag{25a}$$

$$\mathbf{K}_T\left(\mathbf{d}^{(i)}\right) = \left.\frac{\partial \mathbf{K}\left(\mathbf{d}\right)}{\partial \mathbf{d}}\right|_{\mathbf{d}^{(i)}} + \mathbf{K}\left(\mathbf{d}^{(i)}\right) \tag{25b}$$

where $\mathbf{K} = \mathbf{K}_\varepsilon + \mathbf{K}_\varsigma + \mathbf{K}_\eta + \mathbf{K}_\chi$ is the global stiffness matrix. After that, the incremental displacement vector is calculated by

$$\delta\mathbf{d}^{(i)} = -\mathbf{K}_T^{-1}\left(\mathbf{d}^{(i)}\right)\mathbf{R}\left(\mathbf{d}^{(i)}\right) \tag{26}$$

in which $\mathbf{K}_T$ is the tangent stiffness matrix given in details in [56]. After the increment displacement vector $\delta\mathbf{d}^{(i)}$ is computed, the displacement vector at the $(i+1)^{th}$ iteration is computed by

$$\mathbf{d}^{(i+1)} = \mathbf{d}^{(i)} + \delta\mathbf{d}^{(i)} \tag{27}$$

The iterative procedure is terminated when the difference measured using Euclidean norm between the solutions obtained from two consecutive iterations is less than the prescribed tolerance ϵ:

$$\frac{\left\|\mathbf{d}^{(i+1)} - \mathbf{d}^{(i)}\right\|}{\left\|\mathbf{d}^{(i+1)}\right\|} \leq \epsilon \tag{28}$$

For the nonlinear transient analysis of microplates under dynamic loadings, the Newmark's integration scheme [60] is adopted in this study. The initial values of displacements $\mathbf{d}$, velocities $\dot{\mathbf{d}}$ and accelerations $\ddot{\mathbf{d}}$ are prescribed to be zeros. Based on the average acceleration scheme with $\gamma = 1/2$ and $\beta = 1/4$, the increments of displacements, velocities and accelerations between the time step i^{th} and $(i+1)^{th}$ are briefly presented as follows:

$$\Delta\mathbf{d}_i = \hat{\mathbf{K}}^{-1}\Delta\hat{\mathbf{f}}_i \tag{29a}$$

$$\Delta\dot{\mathbf{d}}_i = \frac{\gamma}{\beta\Delta t}\Delta\mathbf{d}_i - \frac{\gamma}{\beta}\dot{\mathbf{d}}_i + \Delta t\left(1 - \frac{\gamma}{2\beta}\right)\ddot{\mathbf{d}}_i \tag{29b}$$

$$\Delta\ddot{\mathbf{d}}_i = \frac{1}{\beta(\Delta t)^2}\Delta\mathbf{d}_i - \frac{1}{\beta\Delta t}\dot{\mathbf{d}}_i - \frac{1}{2\beta}\ddot{\mathbf{d}}_i \tag{29c}$$

where $\hat{\mathbf{K}}$ and $\Delta\hat{\mathbf{f}}_\mathbf{i}$ are the effective global stiffness matrix and the increment force vector, respectively, and Δt denotes the time interval, and

$$\hat{\mathbf{K}} = \mathbf{K} + \frac{1}{\beta(\Delta t)^2}\mathbf{M} \tag{30a}$$

$$\Delta\hat{\mathbf{f}}_\mathbf{i} = \Delta\mathbf{f}_i + \mathbf{a}\dot{\mathbf{d}}_i + \mathbf{b}\ddot{\mathbf{d}}_i \tag{30b}$$

in which

$$\mathbf{a} = \frac{1}{\beta \Delta t}\mathbf{M};\ \ \mathbf{b} = \frac{1}{2\beta}\mathbf{M} \tag{31}$$

For the nonlinear transient analysis, the effective global stiffness matrix $\hat{\mathbf{K}}$ is dependent on the displacement vector at the current time step, and thus the Newton-Raphson iterative procedure is performed for Eq. (29a) with the effective global stiffness matrix $\hat{\mathbf{K}}$ being replaced by the corresponding tangent matrix $\hat{\mathbf{K}}_T$. A flow chart of the proposed program used for transient analysis is given in Fig. 3.

4. Numerical results and discussion

In this section, numerical studies on the nonlinear static bending and transient linear/nonlinear responses of FG microplates are conducted. The following material properties of FG microplates are used henceforward unless otherwise stated: E_m = 1.44×10^9 N/m^2, ρ_m = 1.22×10^3 kg/m^3, E_c = 14.4×10^9, ρ_c = 12.2×10^3 kg/m^3 and $\nu_c = \nu_m$ = 0.38, and the length scale parameter is $\bar{l}$ = 17.6×10^{-6} m. In addition, it is assumed that all three length scale parameters have identical values $l_0 = l_1 = l_2 = l$. Different types of boundary conditions for rectangular plates (SSSS1, SSSS3 and CCCC) and circular plates (Sr and Cr) are considered. Specifications of those boundary conditions are retrieved from [59, 61] and expressed below:

SSSS1

$$u = \theta_x = w = 0 \text{ at } y = 0 \text{ and } y = b \tag{32a}$$

$$v = \theta_y = w = 0 \text{ at } x = 0 \text{ and } x = a \tag{32b}$$

SSSS3

$$u = v = w = 0 \text{ at all edges} \tag{33}$$

CCCC

$$u = v = \theta_x = \theta_y = w = \frac{\partial w}{\partial x} = 0 \text{ at } x = 0 \text{ and } x = a \tag{34a}$$

$$u = v = \theta_x = \theta_y = w = \frac{\partial w}{\partial y} = 0 \text{ at } y = 0 \text{ and } y = b \tag{34b}$$

Sr

$$u = v = w = 0 \tag{35}$$

Cr

$$u = v = \theta_x = \theta_y = w = \frac{\partial w}{\partial n} = 0 \tag{36}$$

where $\frac{\partial w}{\partial n}$ is the the normal derivative operator. It should be noted that the boundary condition relating to the derivative of w is simply treated in the IGA approach by imposing zero values for the transverse displacement in all control points located on the boundaries and those adjacent to them. As discussed in Kim and Reddy [61], the boundary conditions concerning to the symmetric part of rotation tensor should be accounted since they are defined based on the displacement filed. Nevertheless, the effect of those boundary conditions on the results are not much considerable as observed in the Ref. [61].

4.1. Convergence and verification studies

In Table. 1, the results of displacements w/h obtained from different meshes and polynomial orders of B-spline basis functions $(p = q)$ are tabulated. The results are presented for both MCT and MST theories. The microplate in this example is assumed to be square $(h = 2l,\ a = b = 20h,\ l = \bar{l})$, subjected to a uniformly distributed load $q_0 = 5.4\times10^6$ N/m^2, and made from Epoxy, where $E = 1.44\times10^9$ N/m^2, $\nu = 0.38$, $\bar{l} = 17.6\times10^{-6}$ m. The MCT model is obtained by setting the length scale parameters $l_0 = l_1 = 0$. In general, the obtained results converge quickly with the increase of mesh size, and the converged solutions are obtained with a mesh of 16×16 and $p = q = 3$. Therefore, this mesh is used in the remaining calculations. Examples of the 16×16 meshes of circular and rectangular geometries $(p = q = 3)$ are illustrated in Fig. 4.

To verify the accuracy and reliability of the present approach, the nonlinear static bending behaviour of square FG microplates based on the MCT is presented. The obtained results are then compared with those given by Kim and Reddy [61]. Herein, a uniformly distributed load of $q_0 = 5.4\times10^6$ N/m^2 is incrementally applied. The results for SSSS1 and CCCC microplates are plotted in Fig. 5. It is seen that there is a good agreement between the results obtained from the present approach and those from Ref. [61]. The value of $h/l = \infty$ herein denotes the classical case where the size effect is neglected. The results also show that the displacements increase with the increase of the gradient index. Moreover, the results decrease when the ratio h/l becomes smaller since the size effect accordingly becomes more considerable. Fig. 6 compares the nonlinear displacements obtained from the MCT and the MST of a square FG microplate. It can be observed from the results, the displacements obtained from the MST are smaller than that of the MCT. This is due to the fact that the MST involves more additional length scale parameters and more nonlinear components compared to the MCT as mentioned earlier.

In order to prove the reliability of the present approach for the transient analysis, a square orthotropic plate 0.25 m in length and 0.05 m in thickness is considered. It is subjected to a uniform step load with $q_0 = 10^6$ N/m^2. The material properties are given as follows: $E_1 = 525\times10^9$ N/m^2, $E_2 = 525\times10^9$ N/m^2, $G_{12} = G_{13} = G_{23} = 10.5\times10^9$ N/m^2, $\nu_{12} = 0.25$ and $\rho = 800$ kg/m^3. The chosen

time step Δt is 5×10^{-6} s. As depicted in Fig. 7, an excellent agreement between the results obtained from the present approach and those obtained from the finite strip method [62] is archived.

4.2. Parametric study

4.2.1. Nonlinear response of FG microplates under static loadings

In this example, the nonlinear static responses of FG microplates based on the MST are addressed. A uniformly distributed load having intensity of q_0 = 5.4×10^6 N/m^2 is incrementally applied. The influences of gradient index and size effect on the nonlinear responses of FG microplates are depicted in Figs. 8 -10. It is obvious to see that the largest displacements are obtained when a pure metal plate $(n = \infty)$ is considered or when the size effect is dismissed $(h/l = \infty)$. In addition, the displacements decrease by reducing the gradient indices and ratios of h/l or increasing the length scale parameter l. This could be explained that the change of gradient index leads to an increase in the bending stiffness of the plates as more ceramic phrase in the plate volume is given, while the change in length scale parameter results in a greater influence of the size effect. Consequently, the smallest results are obtained when the plate is full ceramic or its sizes are so small that the thickness is equal to or smaller than the length scale parameter. Furthermore, when the size effect becomes most pronounced, e.g. h/l = 1 and 2 or when $l \geq \bar{l}$, it is seen that the response of the plate is almost linear.

The influence of boundary conditions on the nonlinear bending behaviour of FG microplates is illustrated in Fig. 11. It can be seen that the results obtained in the case of immovable simply supported (SSSS3) produces slightly larger results than those in the case of movable counterpart (SSSS1) when $50 \leq \bar{q} \leq 100$ within the current consideration (h/l = 5 and n = 5). However, the SSSS1 boundary condition produces largest displacements in general, followed by the SSSS3 and the CCCC boundary conditions. In Fig. 12, the influence of thickness ratios is also presented. The results obtained from thin to moderately thick plates (a/h = 100 to 20) are not much different to each others. However, the shear deformation effect is clearly observed when thick plates (a/h = 5-10) are considered.

The influences of different loading intensities, gradient indices, size effect and thickness ratios on the stress variations through the plate thickness are illustrated in Figs. 13-16, respectively. In general, the stress profiles vary in accordance with the distributions of the material phrases, whereby the smallest stresses are obtained when a full metal plates is considered. Also, the size effect is observed to play a significant role on the stress results. It is observed that the stresses are reduced remarkable when the size effect is most considerable (see Fig. 15). By increasing the thickness ratio, it is obvious to see that the stresses increases as the general stiffness of the plate is reduced (see Fig. 16). Overall, when the effect of material variations is considered, the larger displacements and

smaller stresses are obtained with greater gradient indices. In addition, it is interesting to see that both displacement and stress results are reduced with the increase of size effect.

4.2.2. Nonlinear response of FG microplates under dynamic loadings

In this section, transient responses of FG microplates under dynamic loadings are analysed. These plates are assumed to be subjected to time-dependent distributed loads, where $q = q_0 \sin\left(\frac{\pi x}{a}\right) \cos\left(\frac{\pi x}{b}\right) F(t)$ for rectangular plates and $q = q_0 F(t)$ for circular plates, q_0 = 2.7×10^6 N/m^2, λ = 10^5 s^{-1}, t_s = 1.5×10^{-5} s, and the time step $\triangle t$ employed herein is 10^{-7} s. Time history of $F(t)$ is depicted in Fig. 17.

$$F(t) = \begin{cases} \begin{cases} 1, & t \leq t_s \\ 0, & t > t_s \end{cases} & \text{Step load} \\ e^{-\lambda t} & \text{Exponential blast load} \end{cases} \tag{37}$$

Figs. 18 -20 illustrate the influences of size effect and geometrical nonlinearity on the transient responses of FG microplates. In general, it can be seen that the linear and nonlinear responses to dynamic loadings are distinguishable, except the cases when h/l = 1 or $l \geq \bar{l}$ where the size effect becomes most pronounced. The nonlinear response generally produces smaller magnitudes of displacement and periods of motion. In addition, the largest discrepancies between linear and nonlinear results are observed in the classical case when the size effect is neglected ($h/l = \infty$). When the influence of the size effect increases, those differences reduce and dismisses at h/l = 1 or $l \geq \bar{l}$. Both magnitudes of displacement and periods of motion decrease with the increase of the size effect. This observation could be explained due to the elevation on bending rigidity of the size effect, which is also discussed in the previous section.

The influences of different gradient indices and geometrical nonlinearity on the dynamic responses of FG microplate are described in Fig. 21. It is seen that the results obtained form the linear and nonlinear analyses are completely different to each other. The magnitudes of displacements and periods of motion obtained from the nonlinear analysis always smaller than those of the linear counterpart, and these differences reduce with the decrease of the gradient index. For both linear and nonlinear results, larger displacement magnitudes are obtained with greater gradient indices since the plates become more flexible. The differences between the periods of motions are not clearly distinguishable in the linear analysis. However, when the nonlinearity is considered, the effect of gradient index are observable whereby larger periods of motion are obtained with smaller gradient indices. The differences between linear and nonlinear results could be attributed to the inclusion of membrane stress in the geometrical stiffness components when the geometrical nonlinearity is accounted.

In order to investigate the influence of boundary conditions on the linear and nonlinear responses, the center displacements of FG microplates with the SSSS1, SSSS3 and CCCC boundary conditions are presented in Fig. 22. It can be observed that the maximum and minimum values of both magnitudes of displacement and periods of motion are obtained in the cases of SSSS1 and CCCC boundary conditions, respectively. Furthermore, the responses of FG microplates with the SSSS1 and SSSS3 boundary conditions are close to each other in linear analysis. However, when the geometrical nonlinearity is considered, the results obtained from these cases are clearly distinguishable. It is also observed in Fig. 22 that the geometrically nonlinear responses of simply supported boundary conditions (SSSS1 and SSSS3) are more considerable than that of clamped one (CCCC). The reason of this phenomenon could be attributed to the fact that clamped boundary condition has more substantial influence on restraining the plates from stretching under external load than the other boundary types.

Finally, the influence of thickness ratios on the transient responses to dynamic loadings is discussed. As depicted in Fig. 23, this effect has a significant influence on both linear and nonlinear responses of FG microplates. The distinctions between the linear and nonlinear results are seen clearly when the plates are relatively thin. For instance, when a/h = 50, there are some minor fluctuations in each period in the nonlinear responses. In addition, the responses obtained from linear and nonlinear analyses are completely different in both frequencies and displacement magnitudes. However, when the plate becomes moderately thick (a/h = 20), the differences between the linear and nonlinear analyses become less considerable, and they are dismissed when the thick plates are considered (a/h = 10). This is due to the fact that the influence of geometrical nonlinearity mainly depends on geometrical stiffness, which plays more important role in thin plates. When it comes to thick plates, the responses of the plates are significant affected by the shear deformation phenomenon and the influence of geometrical stiffness becomes insignificant.

5. Conclusions

An IGA-based numerical approach was successfully developed in this study to investigate the nonlinear responses of FG microplates under static and dynamic loadings. The size effect is accounted based on the MST with three length scale parameters. The third-order shear deformation theory and von Kármán assumption are adopted to account for the shear deformation effect and geometrical nonlinearity. The rule of mixture is also utilized to represent the material variations through the plate thickness. By using the NURBS basis functions, the C^2-continuity requirement is naturally satisfied. The Newton-Raphson iterative procedure and the Newmark's integration scheme are employed to find the nonlinear and transient solutions. The accuracy of present model is proven in the verification studies. Furthermore, numerical results are also presented to investigate the influences of

the size effects, gradient indices, boundary conditions and thickness ratios on the nonlinear behaviour of FG microplates. Finally, some major conclusions are emphasized as follows:

- The IGA approach has been successfully employed to study the geometrically nonlinear problems of FG microplates.
- The size-dependant phenomenon in accordance with the MST plays a considerable role on the geometrically nonlinear responses of microplates. The stiffness of the plates increases remarkably, consequently the obtained results for displacements, stresses and periods of motions are smaller than those obtained form the classical theory.
- The increase of the gradient index produces larger displacements in nonlinear static bending analysis and smaller periods of motions in the nonlinear transient analysis.
- In the transient analysis, the influences of boundary conditions are seen more obviously when the geometrical nonlinearity is considered.
- The influence of thickness ratios on the nonlinear responses of FG microplates is significant, especially for the plates subjected to dynamic loadings.

In conclusion, it can be said that the proposed IGA-based numerical procedure is accurate and robust computational tool for the nonlinear analysis of FG microplates under static and dynamic loadings.

Acknowledgements

This research study was supported by a Postgraduate Research Scholarship at La Trobe University. This financial support is gratefully acknowledged.

Appendix

Details of additional nonlinear components in the strain-displacement matrices are given by

$$\mathbf{B}_g = \begin{bmatrix} 0 & 0 & 0 & 0 & R_{c,x} \\ 0 & 0 & 0 & 0 & R_{c,y} \end{bmatrix}; \mathbf{B}_{g\varsigma} = \begin{bmatrix} 0 & 0 & 0 & 0 & R_{c,xx} \\ 0 & 0 & 0 & 0 & R_{c,yy} \\ 0 & 0 & 0 & 0 & R_{c,xy} \end{bmatrix} \tag{A-1}$$

$$\mathbf{B}_{g\eta} = \begin{bmatrix} 0 & 0 & 0 & 0 & \frac{2}{5}R_{c,xx} - \frac{1}{5}R_{c,yy} \\ 0 & 0 & 0 & 0 & -\frac{1}{5}R_{c,xx} + \frac{2}{5}R_{c,yy} \\ 0 & 0 & 0 & 0 & -\frac{2}{5}R_{c,xy} \\ 0 & 0 & 0 & 0 & -\frac{1}{5}R_{c,xx} + \frac{4}{15}R_{c,yy} \\ 0 & 0 & 0 & 0 & \frac{4}{15}R_{c,xx} - \frac{1}{5}R_{c,yy} \\ 0 & 0 & 0 & 0 & \frac{8}{15}R_{c,xy} \\ 0 & 0 & 0 & 0 & -\frac{1}{5}R_{c,xx} - \frac{1}{15}R_{c,yy} \\ 0 & 0 & 0 & 0 & -\frac{1}{15}R_{c,xx} - \frac{1}{5}R_{c,yy} \\ 0 & 0 & 0 & 0 & -\frac{2}{15}R_{c,xy} \end{bmatrix} \tag{A-2}$$

$$\mathbf{\Lambda}_{\varepsilon} = \begin{bmatrix} w_{,x} & 0 \\ 0 & w_{,y} \\ w_{,y} & w_{,x} \end{bmatrix}; \mathbf{\Lambda}_{\varsigma} = \begin{bmatrix} w_{,xx} & w_{,xy} \\ w_{,xy} & w_{,yy} \end{bmatrix} \tag{A-3}$$

$$\mathbf{\Lambda}_{\eta} = \begin{bmatrix} \frac{2}{5}w_{,xx} - \frac{1}{5}w_{,yy} & -\frac{2}{5}w_{,xy} \\ -\frac{2}{5}w_{,xy} & -\frac{1}{5}w_{,xx} + \frac{2}{5}w_{,yy} \\ 0 & 0 \\ \frac{8}{15}w_{,xy} & \frac{4}{15}w_{,xx} - \frac{1}{5}w_{,yy} \\ 0 & 0 \\ -\frac{1}{5}w_{,xx} + \frac{4}{15}w_{,yy} & \frac{8}{15}w_{,xy} \\ 0 & 0 \\ -\frac{1}{5}w_{,xx} - \frac{1}{15}w_{,yy} & -\frac{2}{15}w_{,xy} \\ 0 & 0 \\ -\frac{2}{15}w_{,xy} & -\frac{1}{15}w_{,xx} - \frac{1}{5}w_{,yy} \end{bmatrix} \tag{A-4}$$

The matrices including inplane stress resultants are presented as follows

$$\hat{\mathbf{N}}_{\varepsilon} = \begin{bmatrix} N_x & N_{xy} \\ N_{xy} & N_y \end{bmatrix}; \hat{\mathbf{N}}_{\varsigma} = \begin{bmatrix} N_x^{\varsigma} & 0 & N_y^{\varsigma} \\ 0 & N_y^{\varsigma} & N_x^{\varsigma} \end{bmatrix} \tag{A-5}$$

$$\hat{\mathbf{N}}_{\eta} = \begin{bmatrix} N_{xxx}^{\eta} & 0 & N_{yyy}^{\eta} & 3N_{xyy}^{\eta} & 0 & 3N_{xxy}^{\eta} & 3N_{xzz}^{\eta} & 0 & 3N_{yzz}^{\eta} \\ 0 & N_{yyy}^{\eta} & N_{xxx}^{\eta} & 0 & 3N_{xxy}^{\eta} & 3N_{xyy}^{\eta} & 0 & 3N_{yzz}^{\eta} & 3N_{xzz}^{\eta} \end{bmatrix} \tag{A-6}$$

References

[1] Koizumi M. The concept of FGM. Ceramic Transactions, Functionally Gradient Materials 1993;34:3–10.

[2] Witvrouw A, Mehta A. The use of functionally graded poly-SiGe layers for MEMS applications. Materials Science Forum 2005;492-493:255–260.

[3] Chong A, Lam D. Strain gradient plasticity effect in indentation hardness of polymers. Journal of Materials Research 1999;14(10):4103–4110.

[4] Liu D, He Y, Tang X, Ding H, Hu P, Cao P. Size effects in the torsion of microscale copper wires: Experiment and analysis. Scripta Materialia 2012;66(6):406–409.

[5] Mcfarland A, Colton J. Role of material microstructure in plate stiffness with relevance to microcantilever sensors. Journal of Micromechanics and Microengineering 2005;15(5):1060–1067.

[6] Mindlin R. Second gradient of strain and surface-tension in linear elasticity. International Journal of Solids and Structures 1965;1(4):417–438.

[7] Eringen A. Nonlocal polar elastic continua. International Journal of Engineering Science 1972;10(1):1–16.

[8] Lim CW, Zhang G, Reddy JN. A higher-order nonlocal elasticity and strain gradient theory and its applications in wave propagation. Journal of the Mechanics and Physics of Solids 2015;78:298–313.

[9] Yang F, Chong A, Lam D, Tong P. Couple stress based strain gradient theory for elasticity. International Journal of Solids and Structures 2002;39(10):2731–2743.

[10] Lam DCC, Yang F, Chong ACM, Wang J, Tong P. Experiments and theory in strain gradient elasticity. Journal of the Mechanics and Physics of Solids 2003;51(8):1477–1508.

[11] Ansari R, Gholami R, Sahmani S. Free vibration analysis of size-dependent functionally graded microbeams based on the strain gradient Timoshenko beam theory. Composite Structures 2011;94(1):221–228.

[12] Akgoz B, Civalek O. Buckling analysis of linearly tapered micro-columns based on strain gradient elasticity. Structural Engineering and Mechanics 2013;48(2):195–205.

[13] Akgoz B, Civalek O. A novel microstructure-dependent shear deformable beam model. International Journal of Mechanical Sciences 2015;99:10–20.

[14] Akgoz B, Civalek O. Bending analysis of FG microbeams resting on Winkler elastic foundation via strain gradient elasticity. Composite Structures 2015;134:294–301.

[15] Norouzzadeh A, Ansari R, Rouhi H. Pre-buckling responses of Timoshenko nanobeams based on the integral and differential models of nonlocal elasticity: an isogeometric approach. Applied Physics A 2017;123(5):330.

[16] Nateghi A, Salamat-talab M. Thermal effect on size dependent behavior of functionally graded microbeams based on modified couple stress theory. Composite Structures 2013;96:97–110.

[17] Ebrahimi F, Barati MR. A nonlocal strain gradient refined beam model for buckling analysis of size-dependent shear-deformable curved FG nanobeams. Composite Structures 2017;159:174–182.

[18] Gholami R, Ansari R. A most general strain gradient plate formulation for size-dependent geometrically nonlinear free vibration analysis of functionally graded shear deformable rectangular microplates. Nonlinear Dynamics 2016;84(4):2403–2422.

[19] Gurses M, Akgoz B, Civalek O. Mathematical modeling of vibration problem of nano-sized annular sector plates using the nonlocal continuum theory via eight-node discrete singular convolution transformation. Applied Mathematics and Computation 2012;219(6):3226–3240.

[20] Nguyen NT, Hui D, Lee J, Nguyen-Xuan H. An efficient computational approach for size-dependent analysis of functionally graded nanoplates. Computer Methods in Applied Mechanics and Engineering 2015;297:191–218.

[21] Phung-Van P, Ferreira AJM, Nguyen-Xuan H, Abdel Wahab M. An isogeometric approach for size-dependent geometrically nonlinear transient analysis of functionally graded nanoplates. Composites Part B: Engineering 2017;118:125–134.

[22] Ansari R, Norouzzadeh A. Nonlocal and surface effects on the buckling behavior of functionally graded nanoplates: An isogeometric analysis. Physica E: Low-dimensional Systems and Nanostructures 2016;84:84–97.

[23] Reddy J, Kim J. A nonlinear modified couple stress-based third-order theory of functionally graded plates. Composite Structures 2012;94(3):1128–1143.

[24] Asghari M, Taati E. A size-dependent model for functionally graded micro-plates for mechanical analyses. Journal of Vibration and Control 2013;19(11):1614–1632.

[25] Liu S, Yu T, Bui TQ. Size effects of functionally graded moderately thick microplates: A novel non-classical simple-FSDT isogeometric analysis. European Journal of Mechanics - A/Solids 2017;66:446–458.

[26] Nguyen HX, Atroshchenko E, Nguyen-Xuan H, Vo TP. Geometrically nonlinear isogeometric analysis of functionally graded microplates with the modified couple stress theory. Computers & Structures 2017;193:110–127.

[27] Nguyen HX, Nguyen TN, Abdel-Wahab M, Bordas SPA, Nguyen-Xuan H, Vo TP. A refined quasi-3d isogeometric analysis for functionally graded microplates based on the modified couple stress theory. Computer Methods in Applied Mechanics and Engineering 2017;313:904–940.

[28] He L, Lou J, Zhang E, Wang Y, Bai Y. A size-dependent four variable refined plate model for functionally graded microplates based on modified couple stress theory. Composite Structures 2015;130:107–115.

[29] Ansari R, Norouzzadeh A, Gholami R, Faghih Shojaei M, Hosseinzadeh M. Size-dependent nonlinear vibration and instability of embedded fluid-conveying SWBNNTs in thermal environment. Physica E: Low-dimensional Systems and Nanostructures 2014;61:148–157.

[30] Ansari R, Gholami R, Norouzzadeh A. Size-dependent thermo-mechanical vibration and instability of conveying fluid functionally graded nanoshells based on Mindlin's strain gradient theory. Thin-Walled Structures 2016;105:172–184.

[31] Ansari R, Gholami R, Norouzzadeh A, Sahmani S. Size-dependent vibration and instability of fluid-conveying functionally graded microshells based on the modified couple stress theory. Microfluid Nanofluid 2015;19(3):509–522.

[32] Thai HT, Vo TP, Nguyen TK, Kim SE. A review of continuum mechanics models for size-dependent analysis of beams and plates. Composite Structures 2017;177:196–219.

[33] Wang B, Zhou S, Zhao J, Chen X. A size-dependent Kirchhoff micro-plate model based on strain gradient elasticity theory. European Journal of Mechanics, A/Solids 2011;30(4):517–524.

[34] Ashoori Movassagh A, Mahmoodi MJ. A micro-scale modeling of Kirchhoff plate based on modified strain-gradient elasticity theory. European Journal of Mechanics - A/Solids 2013;40:50–59.

[35] Mohammadi M, Fooladi Mahani M. An analytical solution for buckling analysis of size-dependent rectangular micro-plates according to the modified strain gradient and couple stress theories. Acta Mechanica 2015;226(10):3477–3493.

[36] Mohammadi M, Fooladi M, Darijani H. Exact boundary conditions for buckling analysis of rectangular micro-plates based on the modified strain gradient theory. International Journal for Multiscale Computational Engineering 2015;13(3):265–280.

[37] Wang B, Huang S, Zhao J, Zhou S. Reconsiderations on boundary conditions of kirchhoff micro-plate model based on a strain gradient elasticity theory. Applied Mathematical Modelling 2015;40(15-16):7303–7317.

[38] Ansari R, Gholami R, Faghih Shojaei M, Mohammadi V, Darabi MA. Thermal buckling analysis of a mindlin rectangular fgm microplate based on the strain gradient theory. Journal of Thermal Stresses 2013;36(5):446–465.

[39] Ansari R, Shojaei MF, Mohammadi V, Gholami R, Rouhi H. Size-dependent thermal buckling and postbuckling of functionally graded annular microplates based on the modified strain gradient theory. Journal of Thermal Stresses 2014;37(2):174–201.

[40] Gholami R, Darvizeh A, Ansari R, Hosseinzadeh M. Size-dependent axial buckling analysis of functionally graded circular cylindrical microshells based on the modified strain gradient elasticity theory. Meccanica 2014;49(7):1679–1695.

[41] Zhang B, He Y, Liu D, Shen L, Lei J. Free vibration analysis of four-unknown shear deformable functionally graded cylindrical microshells based on the strain gradient elasticity theory. Composite Structures 2014;119:578–597.

[42] Ansari R, Gholami R, Faghih Shojaei M, Mohammadi V, Sahmani S. Bending, buckling and free vibration analysis of size-dependent functionally graded circular/annular microplates based on the modified strain gradient elasticity theory. European Journal of Mechanics, A/Solids 2015;49:251–267.

[43] Ansari R, Hasrati E, Faghih Shojaei M, Gholami R, Mohammadi V, Shahabodini A. Size-dependent bending, buckling and free vibration analyses of microscale functionally graded mindlin plates based on the strain gradient elasticity theory. Latin American Journal of Solids and Structures 2016;13(4):632–664.

[44] Sahmani S, Ansari R. On the free vibration response of functionally graded higher-order shear deformable microplates based on the strain gradient elasticity theory. Composite Structures 2013;95:430–442.

[45] Zhang B, He Y, Liu D, Lei J, Shen L, Wang L. A size-dependent third-order shear deformable plate model incorporating strain gradient effects for mechanical analysis of functionally graded circular/annular microplates. Composites Part B: Engineering 2015;79:553–580.

[46] Zhang B, He Y, Liu D, Shen L, Lei J. An efficient size-dependent plate theory for bending, buckling and free vibration analyses of functionally graded microplates resting on elastic foundation. Applied Mathematical Modelling 2015;39(13):3814–3845.

[47] Akgoz B, Civalek O. A microstructure-dependent sinusoidal plate model based on the strain gradient elasticity theory. Acta mechanica 2015;226(7):2277–2294.

[48] Hughes TJR, Cottrell JA, Bazilevs Y. Isogeometric analysis: CAD, finite elements, NURBS, exact geometry and mesh refinement. Computer Methods in Applied Mechanics and Engineering 2005;194(3941):4135–4195.

[49] Nguyen VP, Anitescu C, Bordas SPA, Rabczuk T. Isogeometric analysis: An overview and computer implementation aspects. Mathematics and Computers in Simulation 2015;117:89–116.

[50] Farzam-Rad SA, Hassani B, Karamodin A. Isogeometric analysis of functionally graded plates using a new quasi-3d shear deformation theory based on physical neutral surface. Composites Part B: Engineering 2017;108:174–189.

[51] Nguyen-Thanh N, Zhou K, Zhuang X, Areias P, Nguyen-Xuan H, Bazilevs Y, Rabczuk T. Isogeometric analysis of large-deformation thin shells using RHT-splines for multiple-patch coupling. Computer Methods in Applied Mechanics and Engineering 2017;316:1157–1178.

[52] Tran LV, Phung-Van P, Lee J, Wahab MA, Nguyen-Xuan H. Isogeometric analysis for nonlinear thermomechanical stability of functionally graded plates. Composite Structures 2016;140:655–667.

[53] Shenas AG, Malekzadeh P. Free vibration of functionally graded quadrilateral microplates in thermal environment. Thin-Walled Structures 2016;106:294–315.

[54] Mirsalehi M, Azhari M, Amoushahi H. Buckling and free vibration of the FGM thin microplate based on the modified strain gradient theory and the spline finite strip method. European Journal of Mechanics - A/Solids 2017;61:1–13.

[55] Thai S, Thai HT, Vo TP, Patel VI. Size-dependent behaviour of functionally graded microplates based on the modified strain gradient theory and isogeometric analysis. Computers & Structures 2017;190:219–241.

[56] Thai S, Thai HT, Vo TP, Reddy JN. Post-buckling of functionally graded microplates under mechanical and thermal loads using isogeomertic analysis. Engineering Structures 2017;150:905–917.

[57] Reddy JN. A simple higher-order theory for laminated composite plates. Journal of Applied Mechanics 1984;51(4):745–752.

[58] Cottrell JA, Hughes TJR, Bazilevs Y. Isogeometric Analysis: Toward Integration of CAD and FEA. 1st ed. , Wiley Publishing , 2009.

[59] Reddy JN. An Introduction to Nonlinear Finite Element Analysis. Oxford University Press, New York , 2004.

[60] Newmark NM. A method of computation for structural dynamics. Journal of the Engineering Mechanics Division 1959;85(3):67–94.

[61] Kim J, Reddy JN. A general third-order theory of functionally graded plates with modified couple stress effect and the von karman nonlinearity: theory and finite element analysis. Acta Mechanica 2015;226(9):2973–2998.

[62] Chen J, Dawe DJ, Wang S. Nonlinear transient analysis of rectangular composite laminated plates. Composite Structures 2000;49(2):129–139.

Table 1: Center displacements w/h of rectangular epoxy microplates under uniformly distributed load with different mesh sizes

			$\bar{q} = \frac{q_0 a^4}{Eh^4}$				
Theory	p-order	Mesh	50	100	200	400	600
MCT	3	4×4	0.9234	1.4859	2.1838	3.0332	3.6196
		8×8	0.9213	1.4825	2.1799	3.0314	3.6218
		12×12	0.9213	1.4826	2.1803	3.0325	3.6240
		16×16	0.9213	1.4827	2.1804	3.0327	3.6243
		20×20	0.9213	1.4827	2.1804	3.0327	3.6243
	4	4×4	0.9221	1.4846	2.1838	3.0361	3.6253
		8×8	0.9213	1.4827	2.1803	3.0326	3.6241
		12×12	0.9213	1.4827	2.1804	3.0327	3.6243
		16×16	0.9213	1.4827	2.1804	3.0327	3.6243
		20×20	0.9213	1.4827	2.1804	3.0327	3.6243
MST	3	4×4	0.4926	0.9290	1.6066	2.5016	3.1178
		8×8	0.4915	0.9270	1.6027	2.4954	3.1103
		12×12	0.4915	0.9270	1.6028	2.4957	3.1109
		16×16	0.4915	0.9270	1.6028	2.4958	3.1111
		20×20	0.4915	0.9270	1.6028	2.4958	3.1111
	4	4×4	0.4918	0.9276	1.6045	2.4996	3.1163
		8×8	0.4915	0.9270	1.6029	2.4959	3.1111
		12×12	0.4915	0.9270	1.6028	2.4958	3.1111
		16×16	0.4915	0.9270	1.6028	2.4958	3.1111
		20×20	0.4915	0.9270	1.6028	2.4958	3.1111

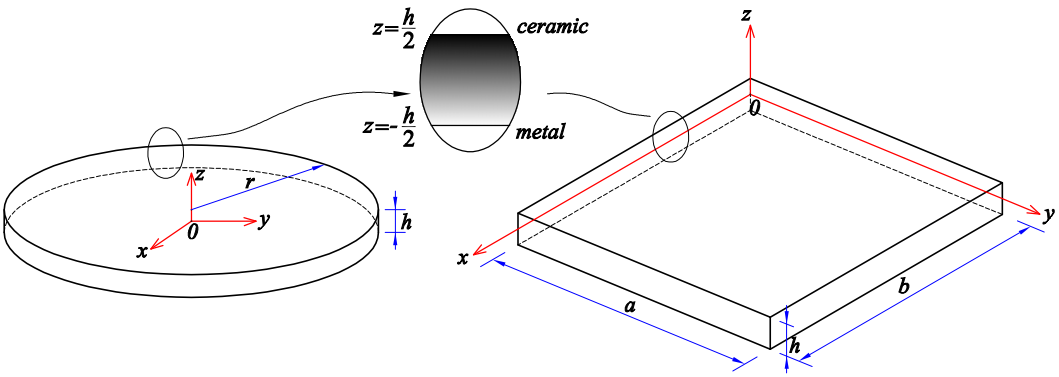

Figure 1: Configurations of rectangular and circular FG microplates

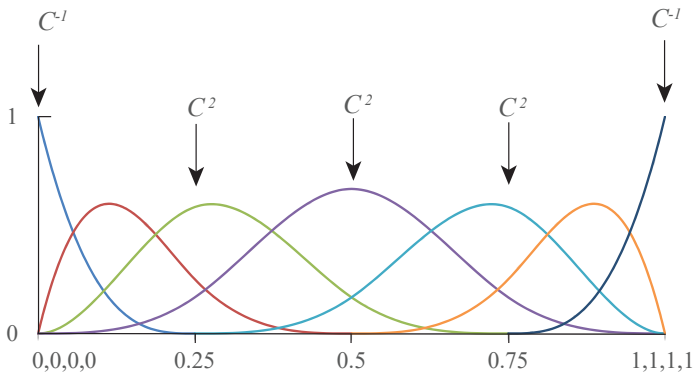

Figure 2: Basic functions with respect to Knot vector $\Xi = \{0, 0, 0, 0, 0.25, 0.5, 0.75, 1, 1, 1, 1\}$

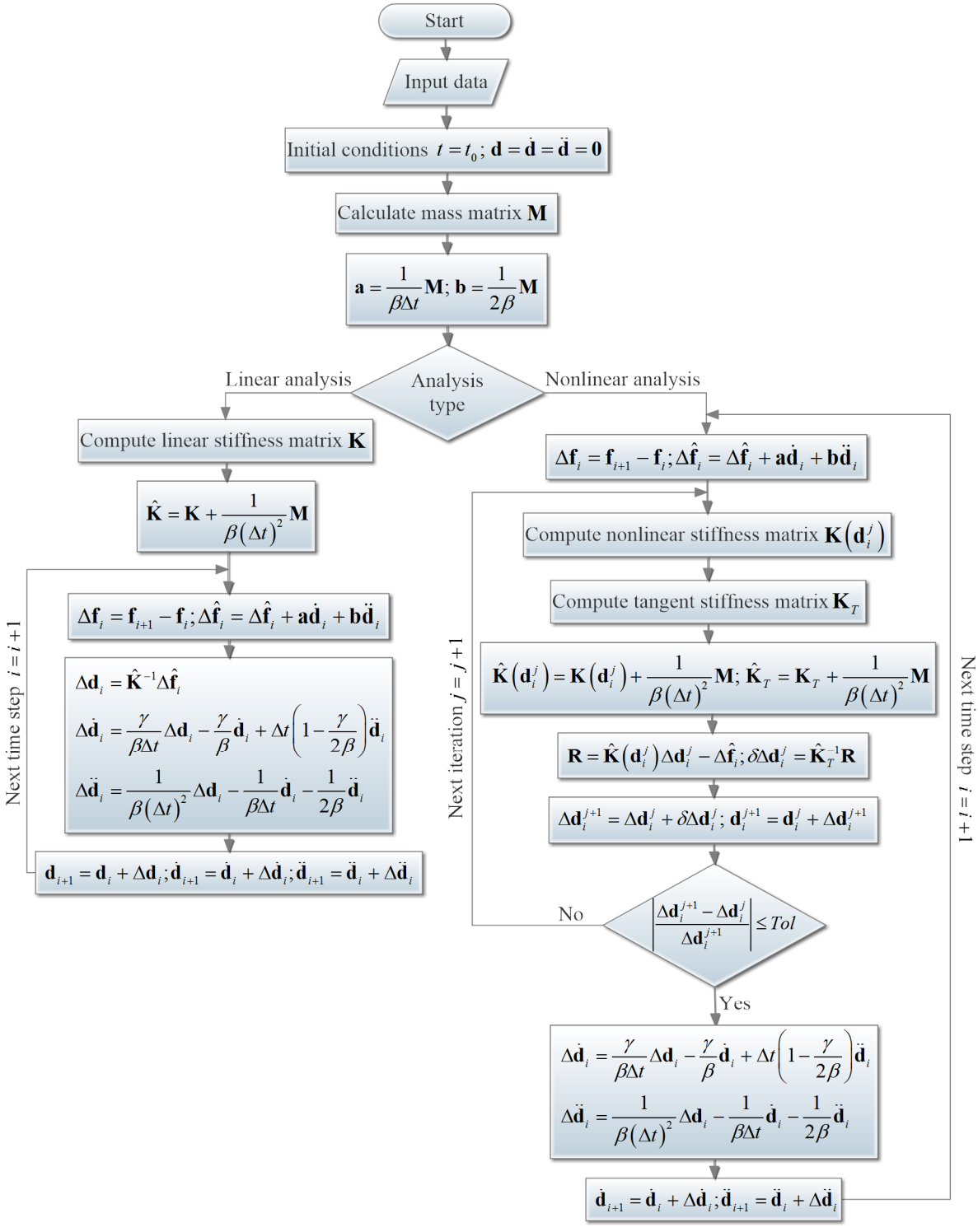

Figure 3: Flowchart of the proposed program used for transient analysis

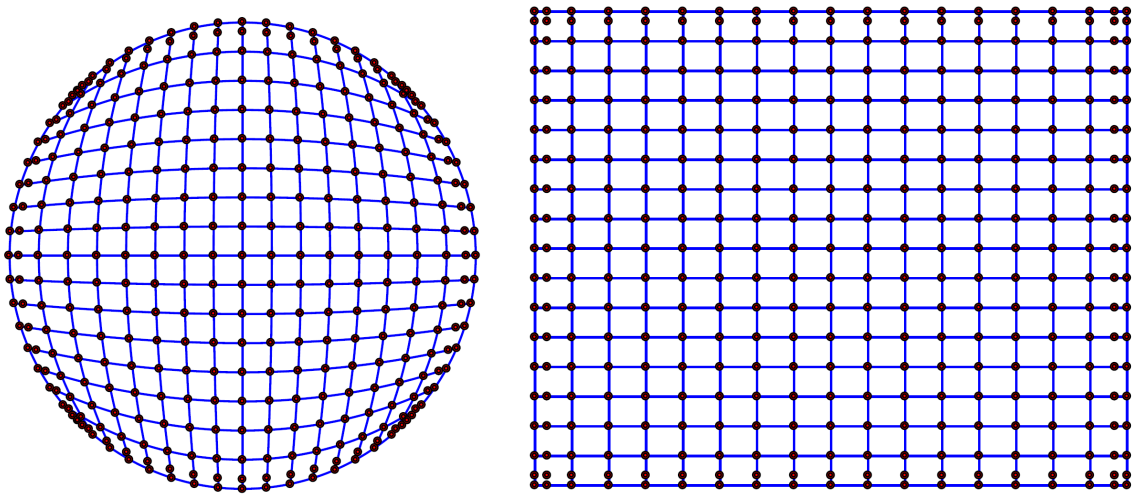

Figure 4: 16×16 meshes of circular and rectangular geometries $(p = q = 3)$

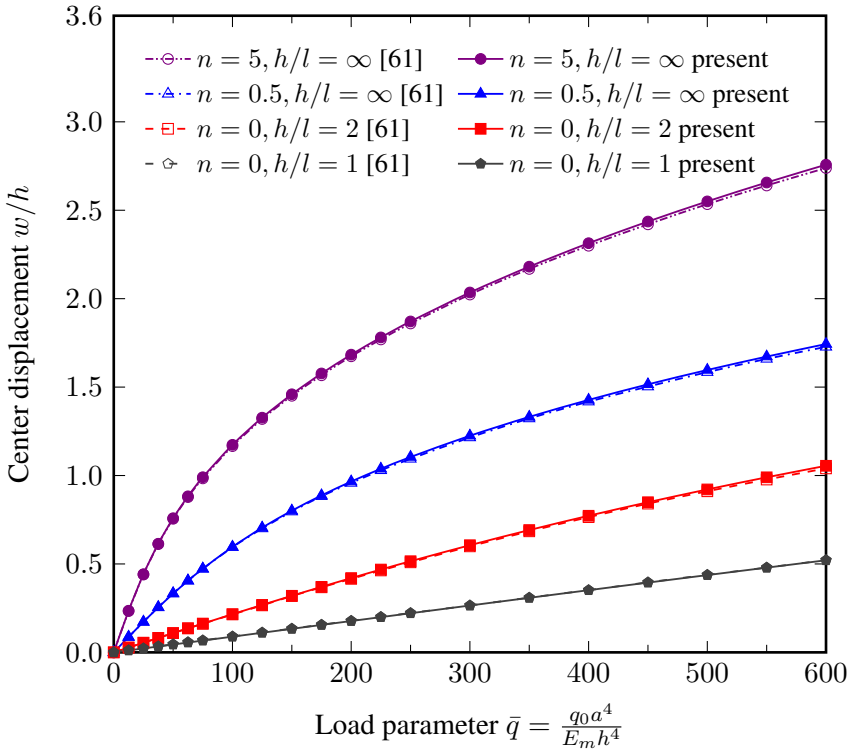

(a) SSSS1

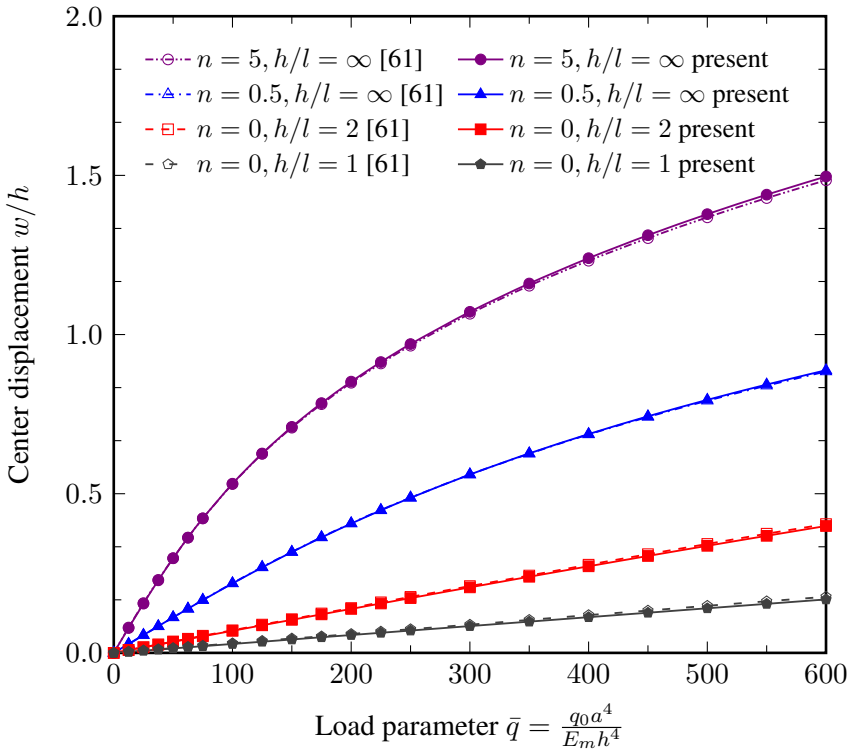

(b) CCCC

Figure 5: Comparisons of nonlinear displacements versus load parameters of square microplates based on the MCT ($l = \bar{l}$)

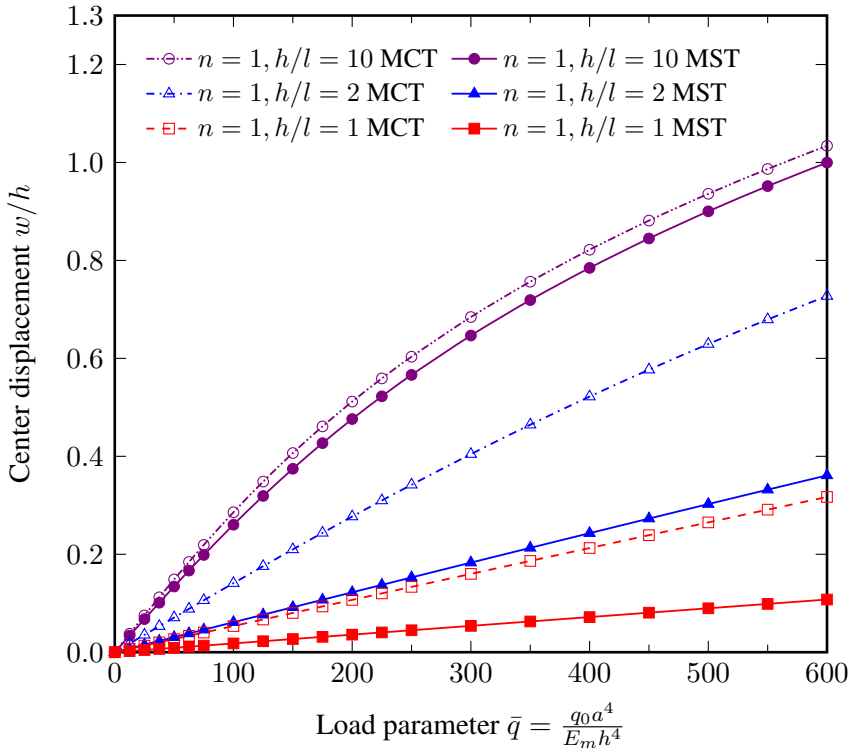

Figure 6: Comparisons between nonlinear displacements of a square CCCC FG microplate obtained from the MCT and MST ($l = \bar{l}$)

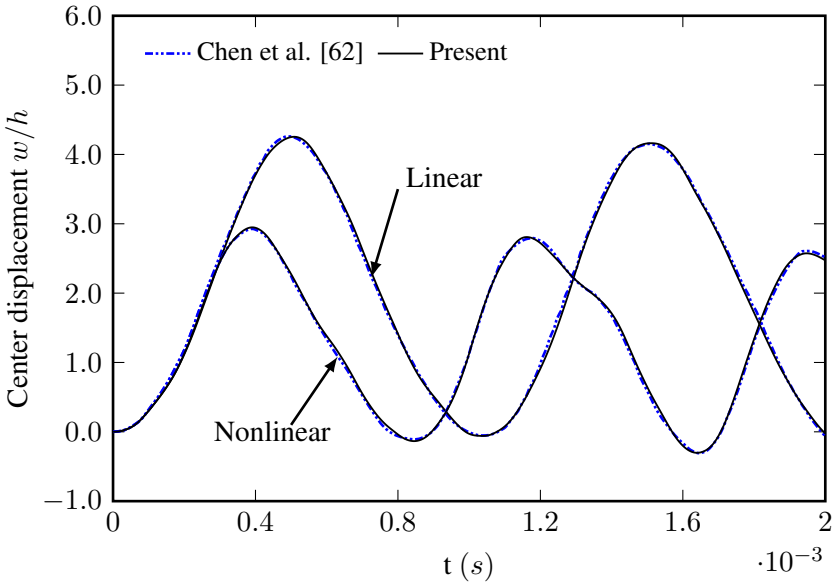

Figure 7: Comparisons the responses of a square orthotropic plate subjected to a uniform step loading

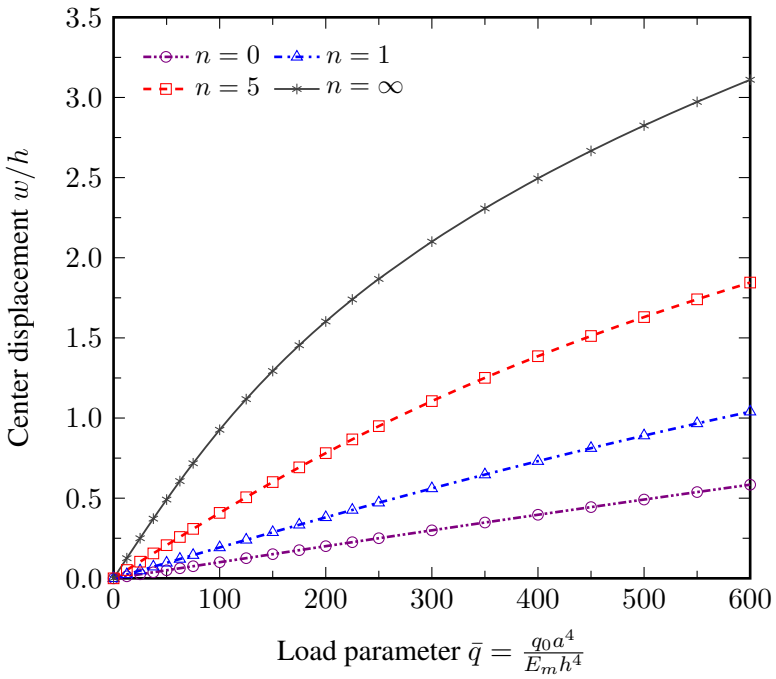

Figure 8: Nonlinear static responses of a square SSSS1 FG microplate with various gradient indices $(h/l = 2, l = \bar{l})$

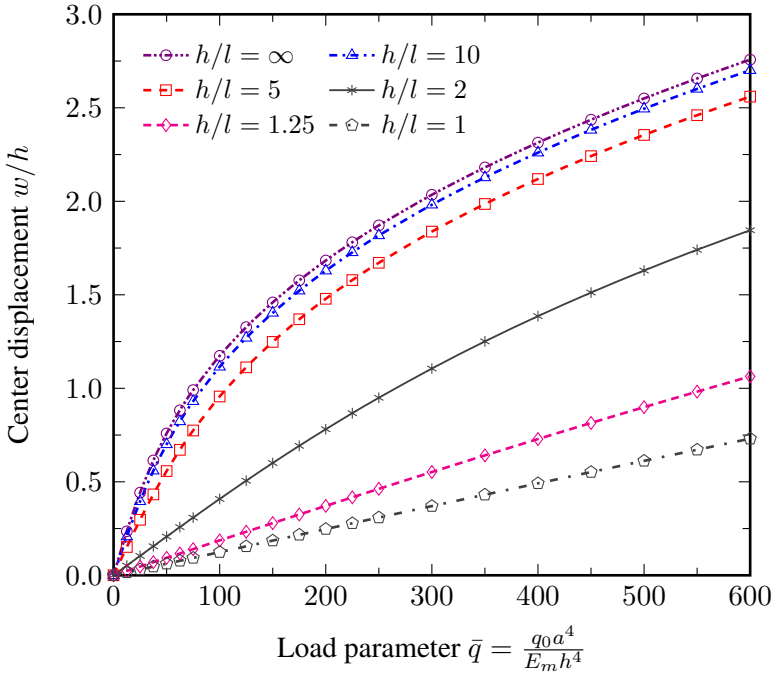

(a) Size effect with various h/l ratios ($l = \bar{l}$)

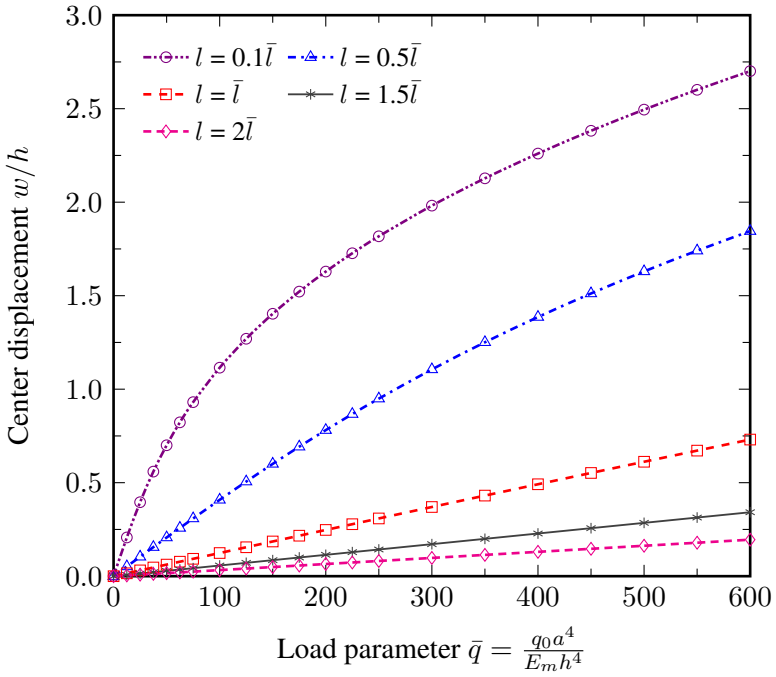

(b) Size effect with various length scale parameters l

Figure 9: Influences of the size effect on the nonlinear static responses of a square SSSS1 FG microplate ($n = 5$)

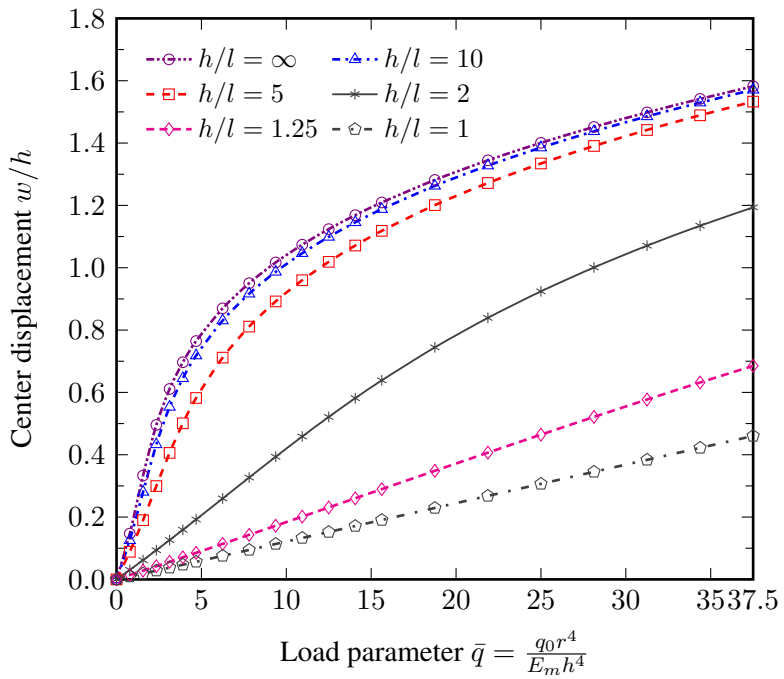

Figure 10: Influences of the size effect on the nonlinear static responses of a circular Sr FG microplate (r = 10h, n = 2, l = $\bar{l}$)

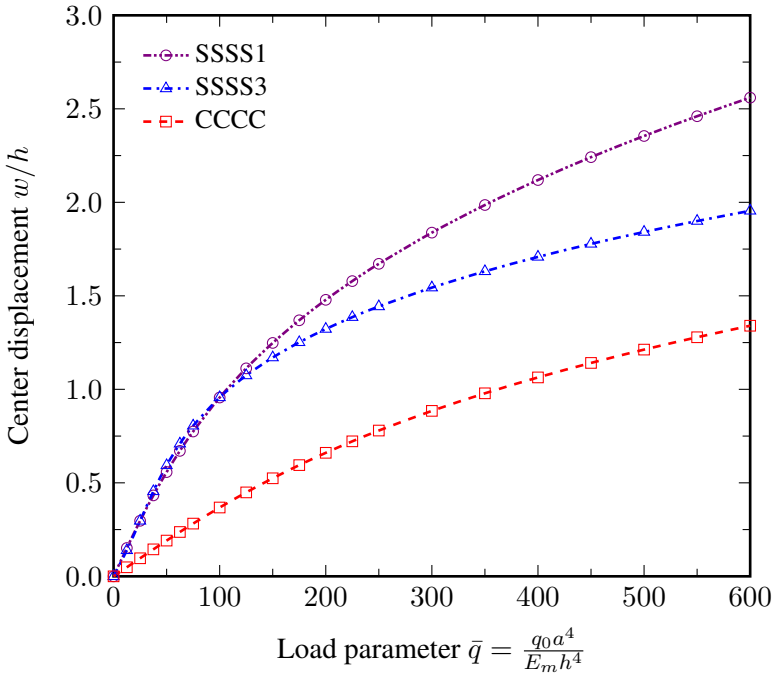

Figure 11: Influences of boundary conditions on the responses of a square FG microplate (h/l = 5, n = 5, $l = \bar{l}$)

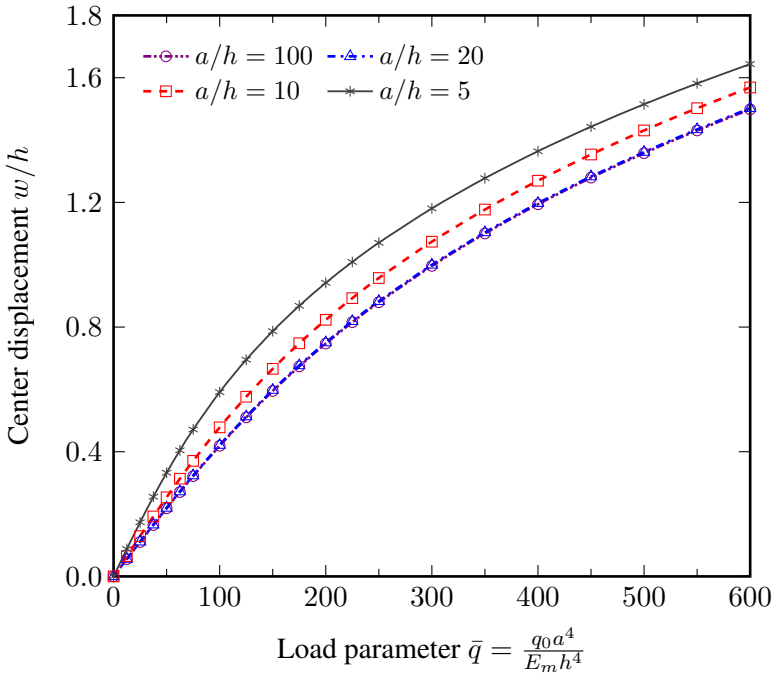

Figure 12: Influences of thickness ratios a/h on the nonlinear responses of a square CCCC microplate (h/l = 10, n = 10, $l = \bar{l}$)

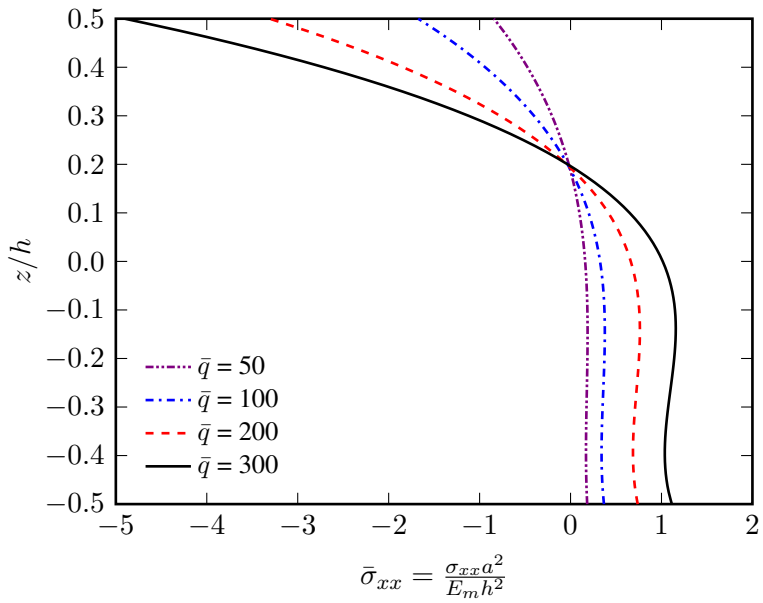

(a) Normal stress $\bar{\sigma}_{xx}\,(a/2, b/2)$

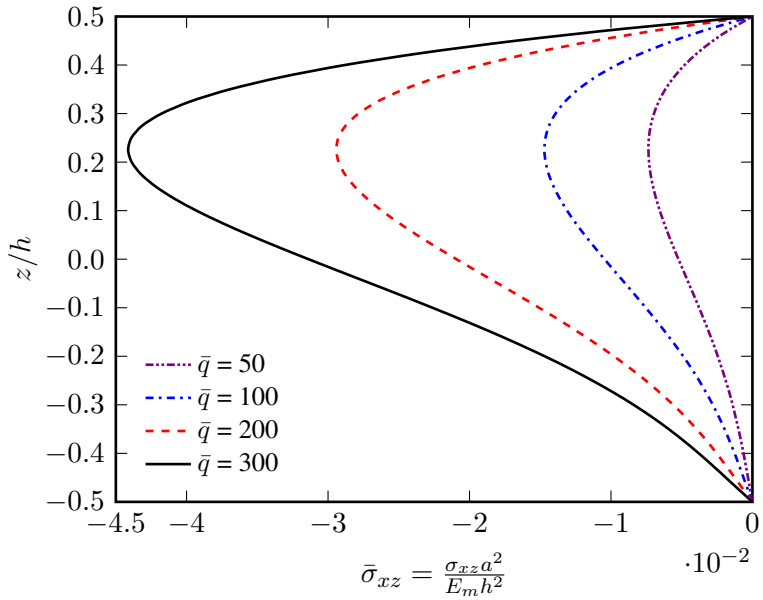

(b) Transverse shear stress $\bar{\sigma}_{xz}\,(0, b/2)$

Figure 13: Influences of the load parameters $\bar{q}$ on the variations of classical stresses through the thickness of a square CCCC FG microplate $(h/l = 1, n = 2, l = \bar{l})$

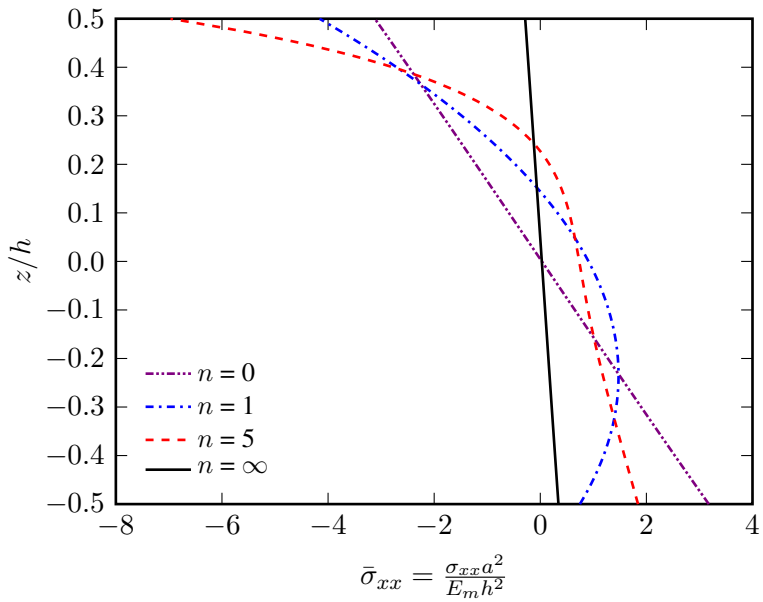

(a) Normal stress $\bar{\sigma}_{xx}\,(a/2, b/2)$

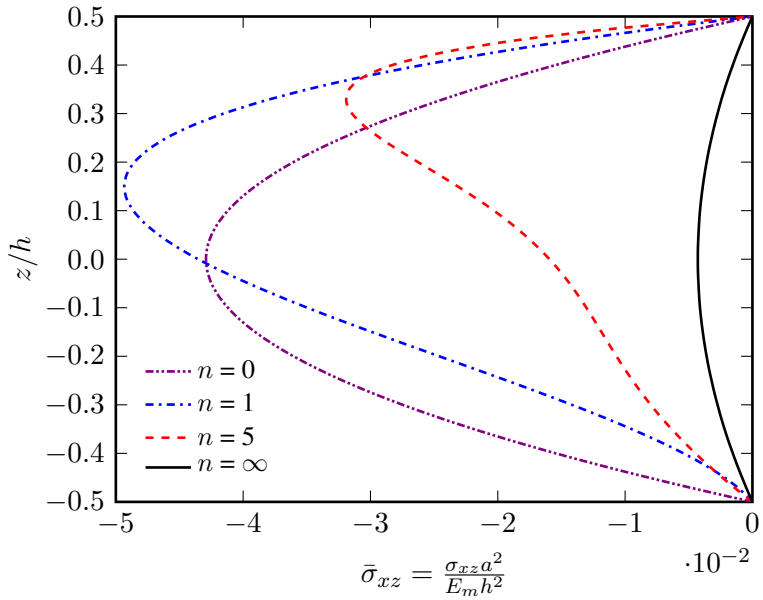

(b) Transverse shear stress $\bar{\sigma}_{xz}\,(0, b/2)$

Figure 14: Influences of the gradient indices on the variations of classical stresses through the thickness of a square CCCC FG microplate ($h/l = 1$, $\bar{q} = 300$, $l = \bar{l}$)

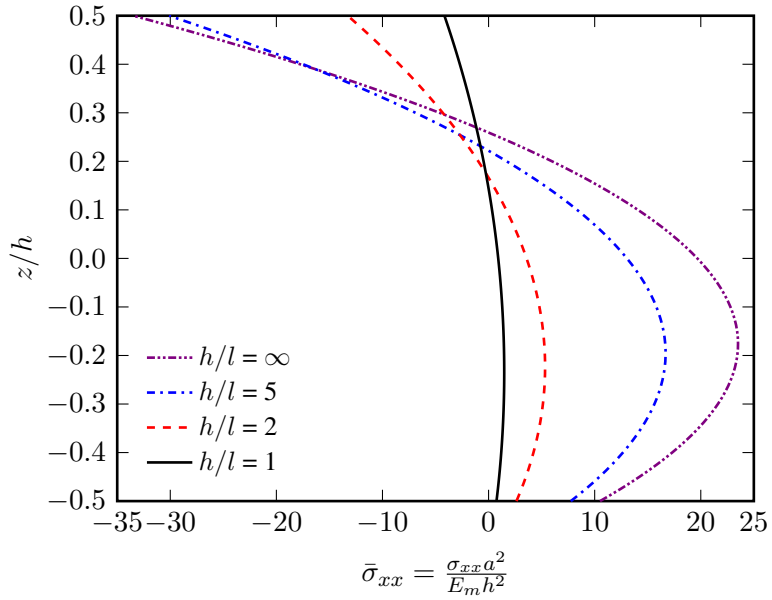

(a) Normal stress $\bar{\sigma}_{xx}\,(a/2, b/2)$

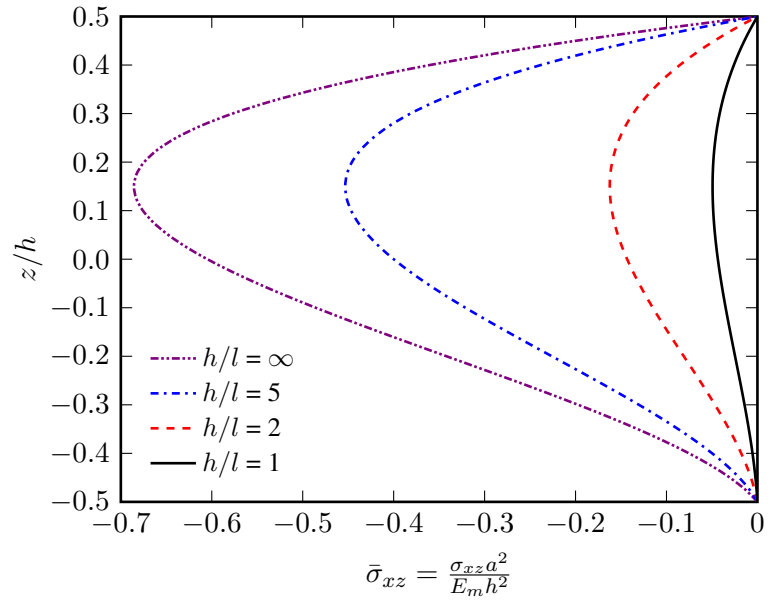

(b) Transverse shear stress $\bar{\sigma}_{xz}\,(0, b/2)$

Figure 15: Influences of the size effects on the variations of classical stresses through the thickness of a square CCCC FG microplate (n = 1, $\bar{q}$ = 300, $l = \bar{l}$)

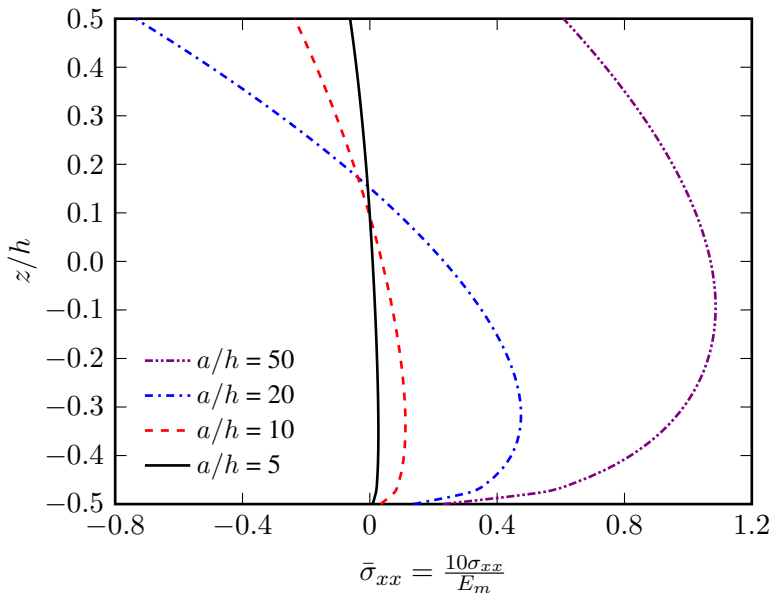

(a) Normal stress $\bar{\sigma}_{xx}$ $(a/2, b/2)$

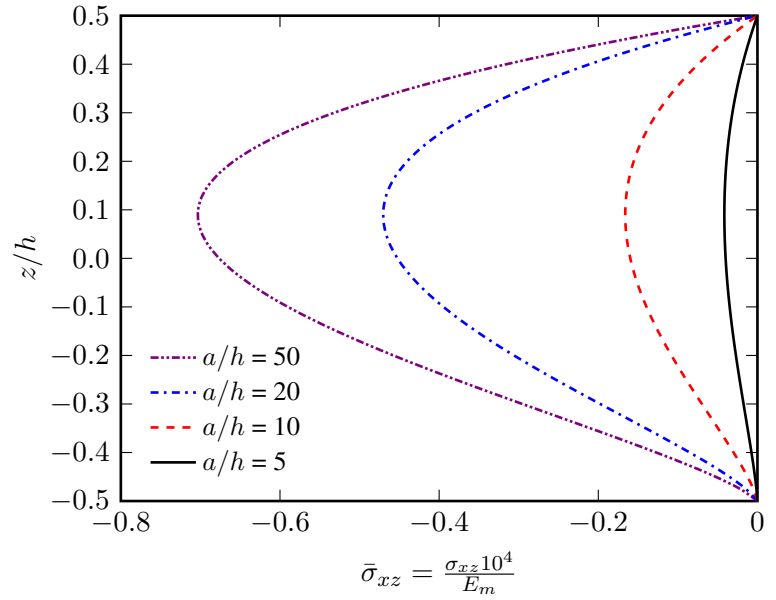

(b) Transverse shear stress $\bar{\sigma}_{xz}$ $(0, b/2)$

Figure 16: Influences of thickness ratios on the variations of classical stresses through the thickness of a square CCCC FG microplate $(n = 0.5,\ h/l = 5,\ q = 0.5q_0,\ l = \bar{l})$

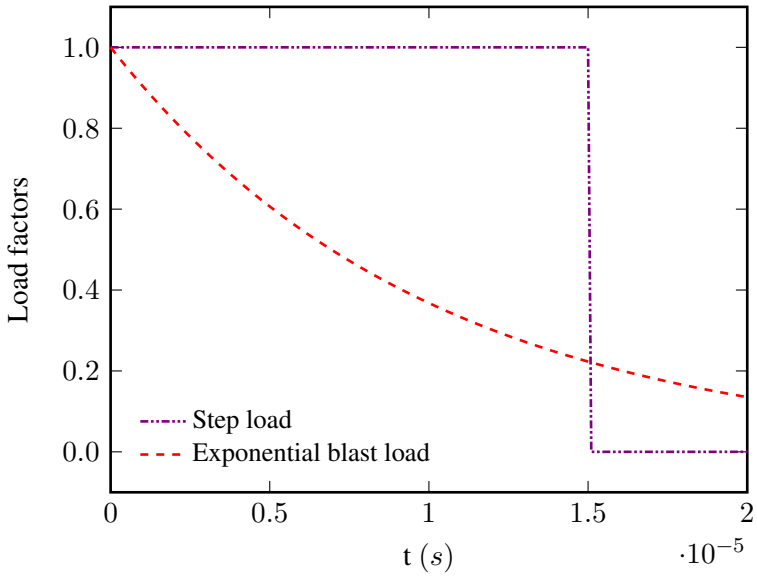

Figure 17: Time history of load factor $F(t)$

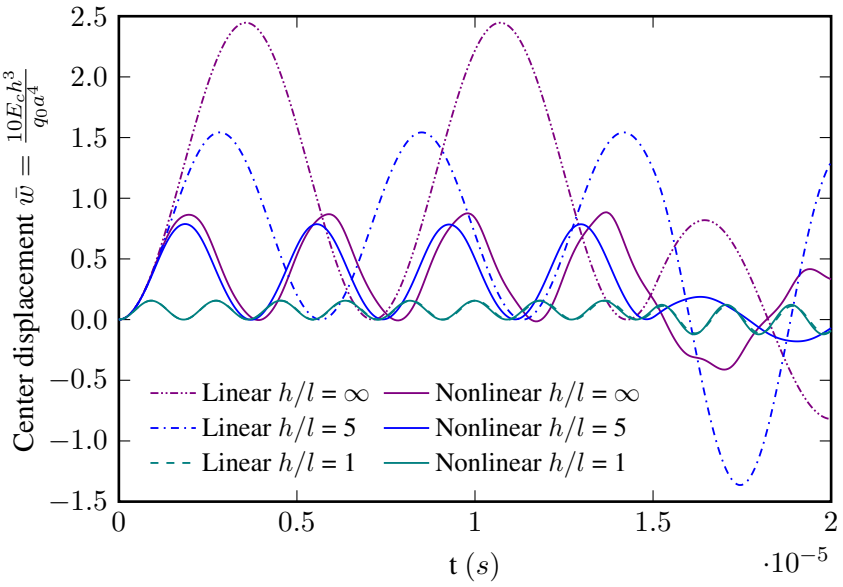

(a) Step load

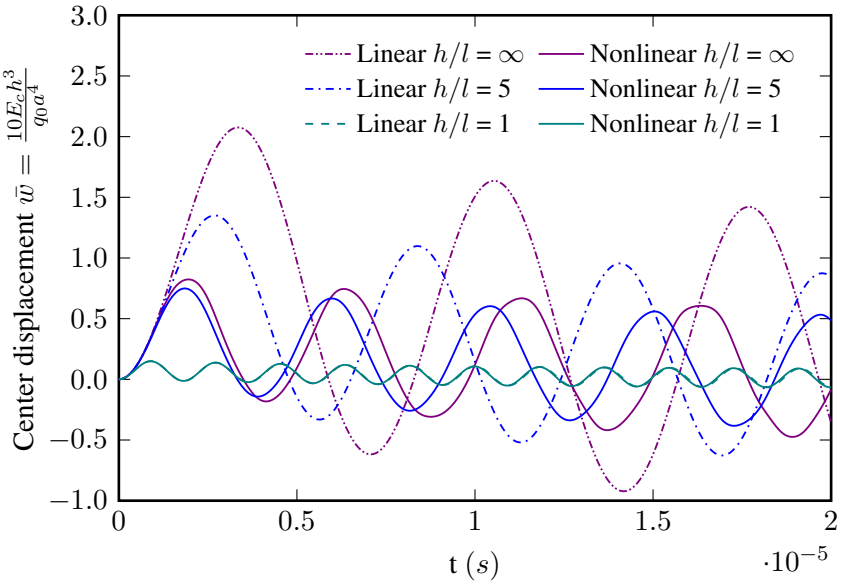

(b) Exponential blast load

Figure 18: Influences of size effect via ratios of h/l on linear and nonlinear responses of a square SSSS1 FG microplate subjected to dynamic loadings $(a/h = 20,\ n = 5,\ l = \bar{l})$

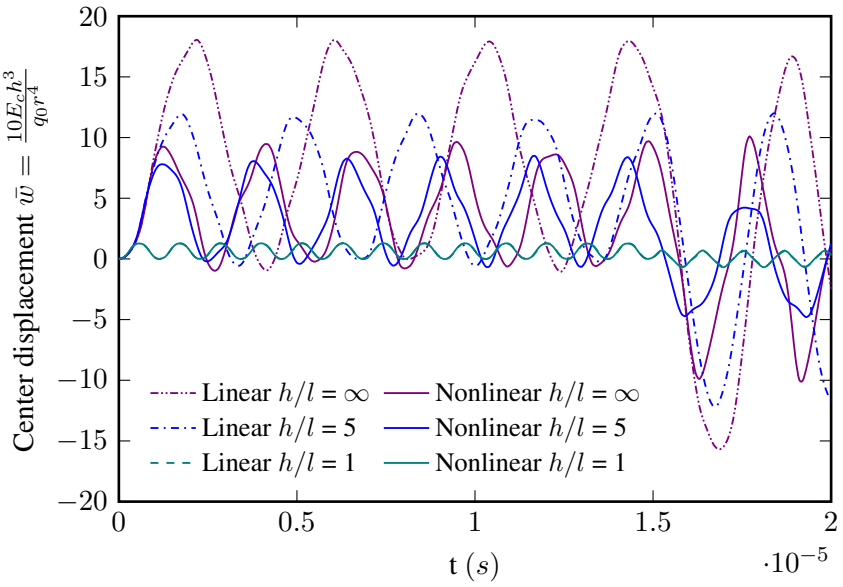

(a) Step load

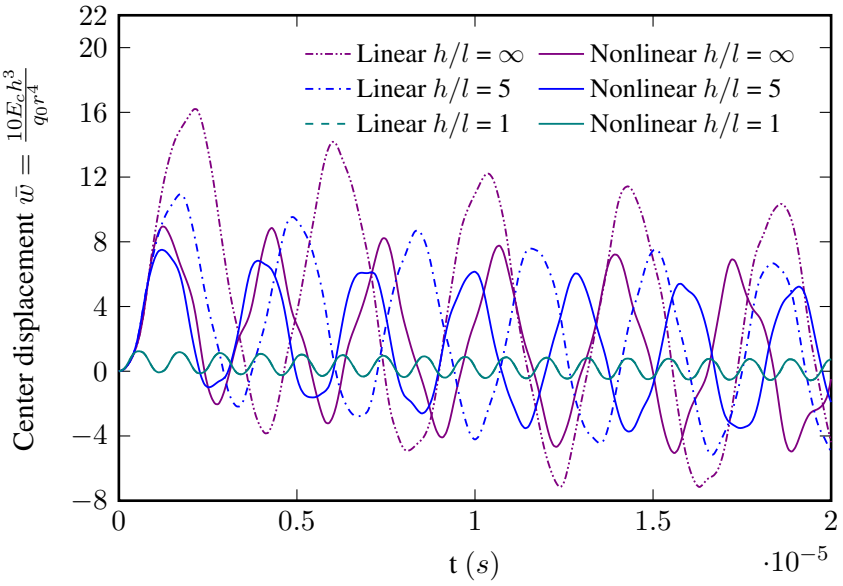

(b) Exponential blast load

Figure 19: Influences of size effect via ratios of h/l on the linear and nonlinear responses of a circular Cr FG microplate subjected to dynamic loadings ($r = 10h$, $n = 10$, $l = \bar{l}$)

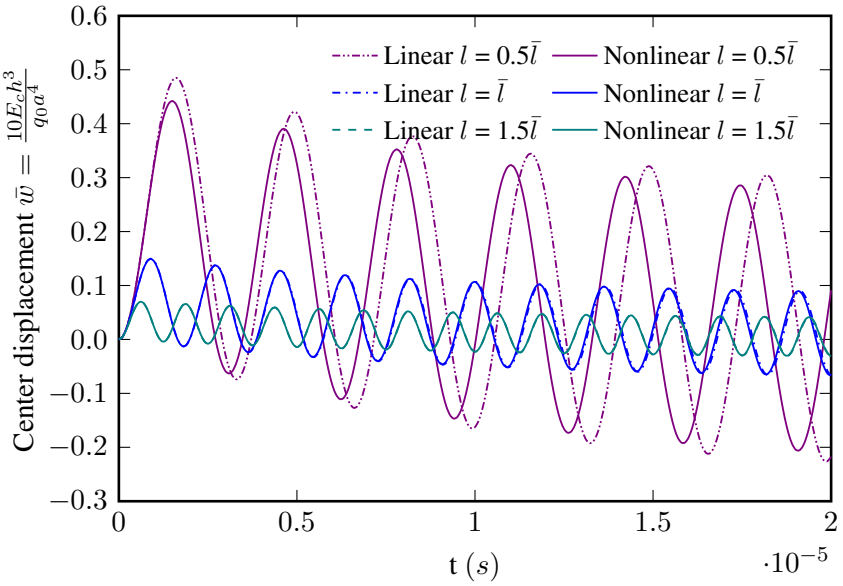

Figure 20: Influences of length scale parameters the linear and nonlinear responses of a square SSSS1 FG microplate subjected to explosive blast load $(a/h = 20, n = 5)$

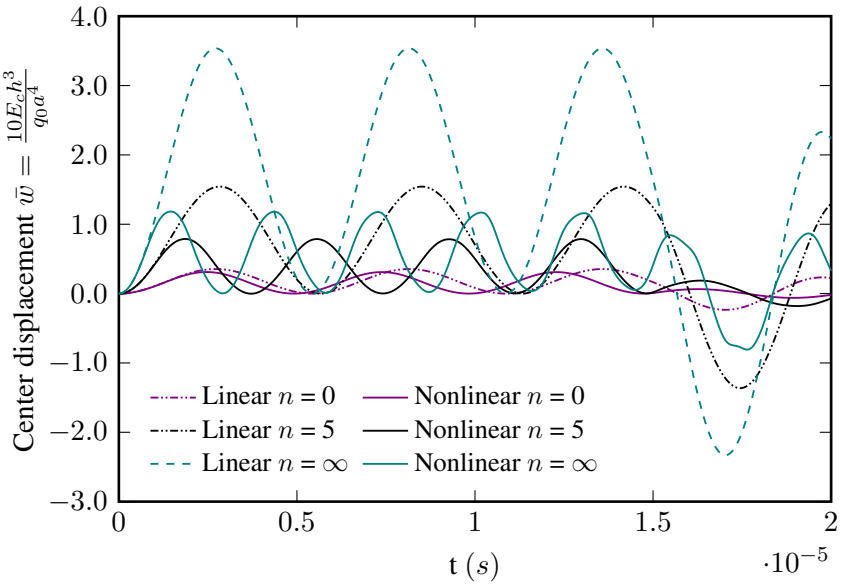

(a) Step load

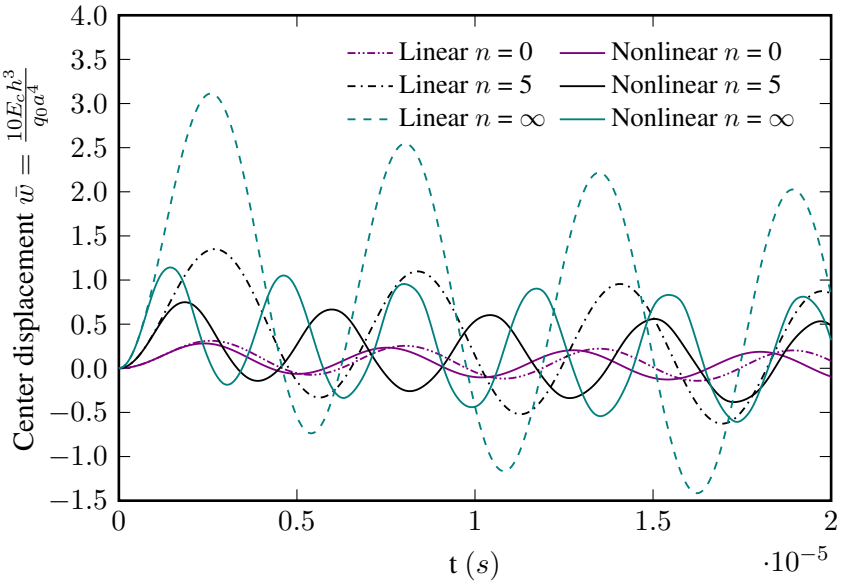

(b) Exponential blast load

Figure 21: Influences of gradient indices on the linear and nonlinear responses of a square SSSS1 FG microplate subjected to dynamic loadings ($h/l = 5$, $a/h = 20$, $l = \bar{l}$)

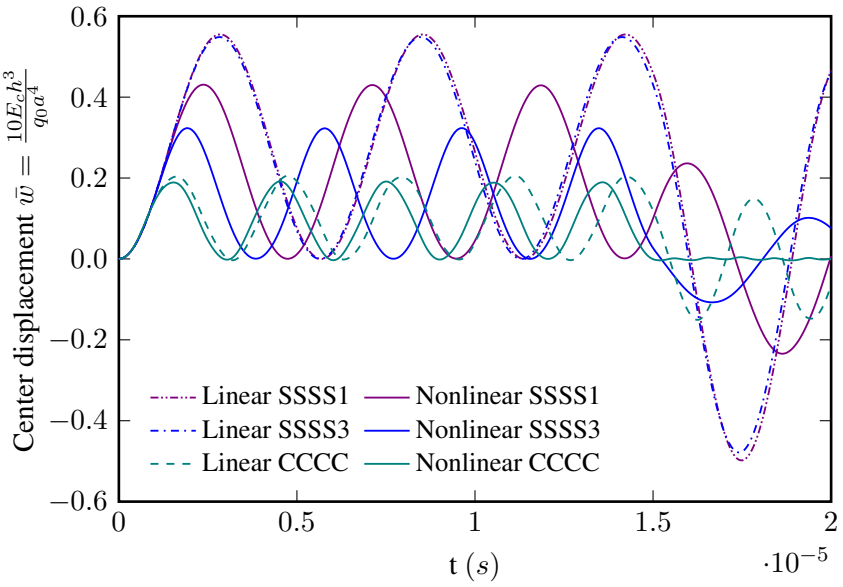

(a) Step load

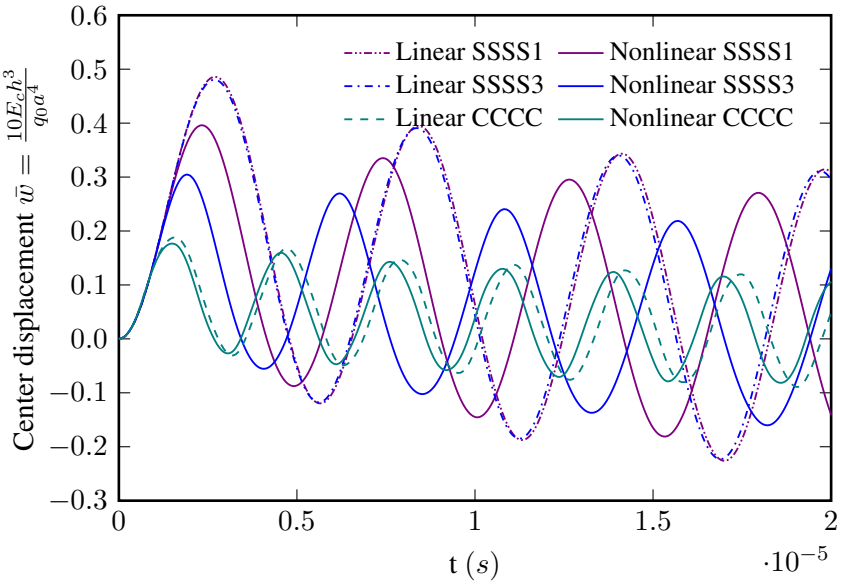

(b) Exponential blast load

Figure 22: Influences of boundary conditions on the linear and nonlinear responses of a square FG microplate subjected to dynamic loadings ($n = 0.5$, $h/l = 5$, $a/h = 20$, $l = \bar{l}$)

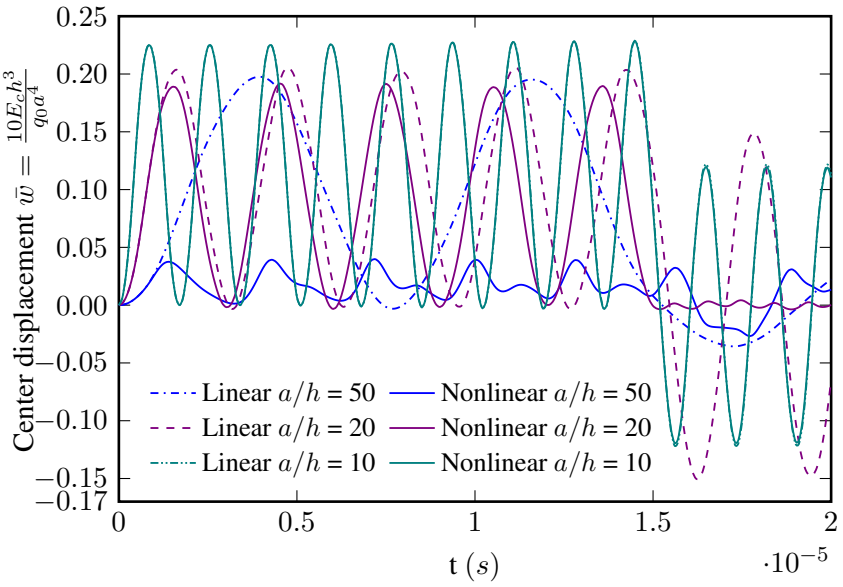

(a) Step load

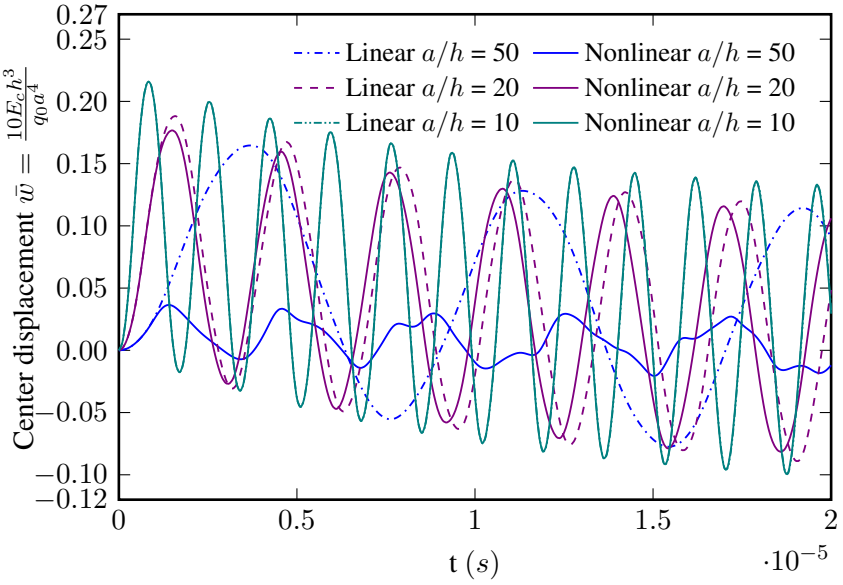

(b) Exponential blast load

Figure 23: Influences of thickness ratios on the linear and nonlinear responses of a square CCCC FG microplate subjected to dynamic loadings (n = 0.5, h/l = 5, $l = \bar{l}$)